DOI: 10.1002/ ((please add manuscript number))

Review

Nanoscale Optical Trapping: a Review

*Carlo Bradac**

C. Bradac

School of Mathematical and Physical Sciences, University of Technology Sydney, Ultimo New South Wales, 2007, Australia

E-mail: carlo.bradac@uts.edu.au

Keywords: optical tweezers, optical trapping, optical forces, nanostructures

Optical trapping is the craft of manipulating objects with light. Decades after its first inception in 1970, the technique has become a powerful tool for ultracold-atom physics and manipulation of micron-sized particles. Yet, optical trapping of objects at the intermediate—nanoscale—range is still beyond full grasp. This matters because the nanometric realm is where several promising advances, from mastering single-molecule experiments in biology, to fabricating hybrid devices for nanoelectronics/photonics, as well as testing fundamental quantum phenomena in optomechanics, are anticipated to produce impactful breakthroughs. After a comprehensive, theoretical introduction to the phenomenon of optical trapping, this review delves into assessing the current state-of-the-art for optical manipulation of objects at the nanoscale. Emphasis is put on presenting the challenges that coalesced into driving the

field to its current development, as well as discussing the outstanding barriers which might lead to future advancements in the field.

1. Introduction

Light carries linear and angular momentum—it can thus exert radiation pressure and torque on physical objects. Yet, the forces from incoherent light are so "minute" that in the first half of the 20th century, physicists found themselves admitting that the practical use of light radiation pressure was "beyond consideration in terrestrial affairs."[1] In 1960, the invention of lasers changed that. A decade later, in 1970, Arthur Ashkin showed that radiation pressure from intense, coherent lasers could accelerate, decelerate, steer and even trap small, micron-sized particles.[2] To some extent serendipitously, Ashkin discovered much more than what his initial intuition suggested.[3] His work set the foundations of *optical trapping*, a field which rapidly developed into two very successful streams of research: on the one hand, laser cooling of single atoms[4-7] and ultracold-atom technologies,[8, 9] and on the other, optical manipulation of micron-sized particles[10-12] and high-sensitive force transduction techniques.[13]

1.1. The First Trap

In 1969, a 'back-of-the-envelope' calculation inspired Ashkin to conduct a simple experiment and determine whether it was feasible to use light radiation pressure to accelerate objects to practical speeds. Photons carry momentum $h\nu/c$ (with h, ν and c being the Planck's constant, the frequency of the photon and the speed of light, respectively). If light from a source with power P shines on a mirror, $P/h\nu$ photons hit the surface every second and transfer a total momentum of $(2P/h\nu)(h\nu/c) = 2P/c$ onto it. A perfectly reflecting mirror should therefore—due to conservation—acquire an equal momentum in the same direction light propagates.

Based on this crude calculations, Ashkin predicted that a light source of power P = 1 W, would produce a force (on an ideally reflecting mirror) of ~10 nN—indeed small in absolute terms.[3] Nevertheless, if a laser beam is used as the light source and is focused on a spot of ~1 μm^2 to hit a particle ~1 μm in diameter, the resulting force does become relevant. Assuming the particle is perfectly reflective and has a density of 1 $g \cdot cm^{-3}$, the calculated acceleration is ~10^9 $cm \cdot s^{-2}$, i.e. roughly 10^6 times the acceleration of gravity. In the experiment Ashkin conducted to test his hypotheses,[2] a cw argon laser (wavelength λ = 514.5 nm, waist radius w_0 = 6.2 μm at the focal point) was employed to accelerate latex spheres (diameter 0.59, 1.31 and 2.68 μm) which were freely suspended in water, in a glass chamber. With just milliwatts of laser power, Ashkin observed that the particles were pushed in the direction of the mildly focused Gaussian laser beam, with values for the acceleration consistent with his rough predictions. Interestingly, he also observed an unanticipated phenomenon. Particles located in the fringes of the beam were drawn towards the beam axis—where the light intensity is the highest—before being accelerated and pushed with ~$\mu m \cdot s^{-1}$ speeds towards the back of the chamber. They would disperse by Brownian motion away from the beam axis once the laser was switched off, yet they would be drawn again towards the centre of the beam upon turning the laser back on—as the radiation pressure had a transverse component to the force, as well as the predicted longitudinal one.

The origin of both the transversal and longitudinal force is usually understood by considering two distinct regimes, depending on the relative size of the particles to the wavelength of the laser beam: the geometrical (ray optics) regime and the Rayleigh (dipole approximation) regime.

1.2. Geometrical (Ray Optics) Regime

The geometrical or ray optics regime is valid for particles whose linear size is far greater than the wavelength of the laser employed as the source of radiation pressure. Photons carry linear

momentum, thus every change in their momentum due to the refraction of light by a transparent object produces a reaction force acting on the object itself. **Figure 1** illustrates the concept. Consider a spherical particle displaced from the beam axis and a pair of light rays, '1' and '2', striking the particle symmetrically with respect to its centre (Figure 1a). Neglecting minor surface reflections, the rays refract through the particle and produce the forces F_1 and F_2. The longitudinal components of F_1 and F_2 have the same direction and they sum to produce the *scattering* force, F_{scatt}, in the direction of the beam. Conversely, the transversal components of F_1 and F_2—orthogonal to the beam axis—have opposite direction. Owing to the relative position of the rays with respect to the intensity profile of the laser beam, the transversal component of F_1 is smaller than that of F_2. The resulting transversal *gradient* force, F_{grad}, points towards the high intensity region of the laser (F_{grad} = 0 when the particle lies on the beam axis, as the transversal components of F_1 and F_2 cancel each other out). Note that for a low-index particle placed off-axis, the refraction reverses (in effect, the particle behaves like a diverging lens rather than a converging one). The force F_1 is greater than F_2 and the particle is pushed away from the beam. This has been verified with micron-sized air bubbles in a mixture of glycerol and water.[2]

An exact expression for the scattering and gradient forces F_{scatt} and F_{grad}, can be derived by means of the Fresnel equations for reflection and transmission. Consider a single ray of power P hitting a particle with an incident angle θ and momentum n_mP/c (n_m being the refractive index of the medium and c the speed of light). The total force on the sphere is the sum of contribution for the reflected ray of power PR and the infinite number of refracted rays of successively decreasing power PT^2, PT^2R, ..., PT^2R^N, etc. (Figure 1a, inset, top). The quantities R and T are the Fresnel reflection and transmission coefficients of the surface at the reflection and transmission angles θ_R and θ_T of the incident rays. This analysis produces the following expression for F_{scatt} and F_{grad}:[14]

$$F_{scatt} = \sum_{i}^{N} \frac{n_m \cdot P_i}{c} \left(1 + R_i \cos(2\vartheta_{R_i}) - \frac{T_i^2[\cos(2\vartheta_{R_i} - 2\vartheta_{T_i}) + R_i \cos(2\vartheta_{R_i})]}{1 + R_i^2 + 2R_i \cos(2\vartheta_{T_i})} \right) \quad (1)$$

$$F_{grad} = \sum_{i}^{N} \frac{n_m \cdot P_i}{c} \left(1 + R_i \sin(2\vartheta_{R_i}) - \frac{T_i^2[\sin(2\vartheta_{R_i} - 2\vartheta_{T_i}) + R_i \cos(2\vartheta_{R_i})]}{1 + R_i^2 + 2R_i \cos(2\vartheta_{T_i})} \right) \quad (2)$$

The formulas sum over all scattered rays. The forces are polarization dependent as *R* and *T* are different for rays polarized perpendicularly or parallel to the plane of incidence.

Ashkin's unanticipated observation of the transversal component of the laser radiation pressure, led to the design of the first 3D particle trap. The trap consisted of two counter-propagating and mildly diverging Gaussian beams focused at points f_1 and f_2 (Figure 1a, inset, bottom). Any radial displacement of the particle away from the beam axis is opposed by the gradient forces of both lasers, directed towards the axis. The longitudinal displacement is null as the scattering forces of the two opposite lasers cancel each other out. The particle is thus drawn towards the equilibrium point between the two beams.

Interestingly, even when a single beam is employed a backward net gradient force can arise due to the refraction of light (Figure 1b).[14] This occurs when the laser is tightly focused, for instance by means of a high-numerical-aperture (NA) objective. In the case of a single-beam trap, the scattering and the gradient forces can still be obtained from Equation 1 and 2—considered as vector sums of the corresponding components for each individual ray. For very high angles of incidence the backward net force can overcome the scattering one, effectively keeping the particle trapped at the focus.

1.3. Rayleigh (Dipole Approximation) Regime

The Rayleigh or dipole approximation regime applies when the diameter of the object is decidedly smaller than the wavelength of light. Irrespective of the object being a small dielectric particle or a single atom/molecule, a general expression of the optical forces can be derived by considering the interaction of the (inhomogeneous) electromagnetic field of the

laser beam with the object itself—treated as a point dipole. From the general expression, the cases for dielectric particles (classical approach) and for single atoms/molecules (semi-classical approach) can be analysed separately as they carry their own specificities.

Consider the general case of a dipole consisting of two opposite charges with masses M_1 and M_2, separated by distance $|d|$ and interacting with arbitrary electric and magnetic fields $\vec{E}$ and $\vec{B}$ (**Figure 2a**). The equations of motion (in the nonrelativistic limit) for the two particles are:

$$M_1\ddot{\vec{r}}_1 = q\left[\vec{E}(\vec{r}_1,t) + \dot{\vec{r}}_1 \times \vec{B}(\vec{r}_1,t)\right] - \nabla U_b(\vec{r}_1,t) \tag{3}$$

$$M_2\ddot{\vec{r}}_2 = -q\left[\vec{E}(\vec{r}_2,t) + \dot{\vec{r}}_2 \times \vec{B}(\vec{r}_2,t)\right] + \nabla U_b(\vec{r}_2,t) \tag{4}$$

where the dots indicate differentiation with respect to time. The first two terms account for the electric and magnetic force (Lorentz Force) on each point charge; U_b is the binding energy between the two particles. The electric field at the position of each particle can be written as the Taylor series expansion:

$$\vec{E}(\vec{r}_1) = \sum_{n=0}^{\infty} \frac{1}{n!}\left[(\vec{r}_1 - \vec{r})\cdot\nabla\right]^n \vec{E}(\vec{r}) = \vec{E}(\vec{r}) + (\vec{r}_1 - \vec{r})\cdot\nabla\vec{E}(\vec{r}) + \ldots \tag{5}$$

$$\vec{E}(\vec{r}_2) = \sum_{n=0}^{\infty} \frac{1}{n!}\left[(\vec{r} - \vec{r}_2)\cdot\nabla\right]^n \vec{E}(\vec{r}) = \vec{E}(\vec{r}) - (\vec{r}_2 - \vec{r})\cdot\nabla\vec{E}(\vec{r}) + \ldots \tag{6}$$

where $\vec{r}$ is the centre of mass coordinate:

$$\vec{r} = \frac{M_1}{M_1 + M_2}\vec{r}_1 + \frac{M_2}{M_1 + M_2}\vec{r}_2 \tag{7}$$

Analogous expressions to 5 and 6 can be written for the magnetic field, $\vec{B}(\vec{r}_1)$ and $\vec{B}(\vec{r}_2)$. For $|d| = |\vec{r}_1 - \vec{r}_2| << \lambda$, with λ being the wavelength of the radiation field, the expansions in 5 and 6 can be truncated at the second term (dipole approximation). Using Equations 3–7 and the definition $\vec{p} = q\vec{d}$ for the dipole moment, the formula for the total force $\vec{F} = (M_1 + M_2)\ddot{\vec{r}}$, acting on the system of two particles, yields:

$$\vec{F} = (\vec{p}\cdot\nabla)\vec{E} + \dot{\vec{p}} \times \vec{B} + \dot{\vec{r}} \times (\vec{p}\cdot\nabla)\vec{B}, \tag{8}$$

where the dependence $(\vec{r},t)$ has been omitted for clarity, and the parenthesis in $(\vec{p}\cdot\nabla)\vec{E}$ and $(\vec{p}\cdot\nabla)\vec{B}$ indicate that the inner product $\vec{p}\cdot\nabla=(p_x,p_y,p_z)\cdot(\partial/\partial x,\partial/\partial y,\partial/\partial z)$ has to be evaluated prior to $\vec{E}$ and $\vec{B}$. Equation 8 shows that the force due to the electromagnetic field acting on a dipole consists of three main terms. The first and last terms originate from the interaction with an inhomogeneous electric and magnetic field, respectively; the second term is instead due to the (magnetic) Lorentz force. The last term is usually much smaller than the other two and can be omitted. Note that, whilst quite general, in this derivation the fields $\vec{E}$ and $\vec{B}$ are, strictly, the exciting fields—i.e. it is assumed that the dipole does not change the fields.

1.3.1. Generalized Expression of the Force

To derive the basic equations for a particle within an optical trap, we consider the case of a simple oscillator subject to a classical radiation field. In Equation 8, the second term can be written as:

$$\begin{aligned}\dot{\vec{p}}\times\vec{B} &= -\vec{p}\times\frac{d}{dt}\vec{B}+\frac{d}{dt}(\vec{p}\times\vec{B})= \\ &= \vec{p}\times(\nabla\times\vec{E})+\frac{d}{dt}(\vec{p}\times\vec{B})\end{aligned} \tag{9}$$

where $d\vec{B}/dt$ is approximated by $\partial\vec{B}/\partial t$, as the velocity of the centre of mass is assumed small compared to the speed of light *c*, and Maxwell's equation $\nabla\times\vec{E}=-\partial\vec{B}/\partial t$ is used. Employing Equation 9 and omitting the third, negligible term in 8 the equation for the force becomes:

$$\vec{F}=\sum_{i=x,y,z}p_i\nabla E_i+\frac{d}{dt}(\vec{p}\times\vec{B}) \tag{10}$$

where the last term vanishes in the time average, yielding:

$$\left\langle\vec{F}\right\rangle=\sum_{i=x,y,z}\left\langle p_i(t)\nabla E_i(t)\right\rangle \tag{11}$$

Given an electromagnetic wave with angular frequency ω and corresponding fields $\vec{E}(\vec{r},t)=\mathrm{Re}\{\underline{\vec{E}}(\vec{r})e^{-i\omega t}\}$ and $\vec{B}(\vec{r},t)=\mathrm{Re}\{\underline{\vec{B}}(\vec{r})e^{-i\omega t}\}$, if there is a linear relationship between dipole and fields, the dipole oscillates at the same driving frequency ω: $\vec{p}(t)=\mathrm{Re}\{\underline{\vec{p}}\,e^{-i\omega t}\}$. In these expressions the underline represents complex amplitudes. Assuming the particle has no static dipole moment, to first order, the induced dipole moment is proportional to the electric field at the particle position ($\vec{r}_0$) through its polarizability α (which depends on the angular frequency ω):

$$\underline{\vec{p}}=\alpha(\omega)\underline{\vec{E}}(\vec{r}_0) \tag{12}$$

Generally the polarizability α is a tensor of rank two. However for atoms and molecules a scalar representation is often sufficient as what matters is the projection of $\vec{p}$ along the direction of the electric field. Using Equation 12, Equations 8 and 11 become:

$$\left\langle \vec{F} \right\rangle=\frac{1}{2}\mathrm{Re}\left\{(\underline{\vec{p}}^{\,*}\cdot\nabla)\underline{\vec{E}}-i\omega(\underline{\vec{p}}^{\,*}\times\underline{\vec{B}})\right\} \tag{13}$$

$$\left\langle \vec{F} \right\rangle=\sum_{i=x,y,z}\frac{1}{2}\mathrm{Re}\left\{\underline{p}_i^{*}\nabla\underline{E}_i\right\}=\sum_{i=x,y,z}\frac{1}{2}\mathrm{Re}\left\{\alpha(\omega)\underline{E}_i(\vec{r})\partial^i\underline{E}_i^{*}(\vec{r})\right\} \tag{14}$$

Using the linear relationship in 12 and representing the field in the paraxial form—either a beam or a plane wave (propagating/evanescent) such that it has a main propagation direction $\vec{k}$—the light field can be written as $\underline{\vec{E}}(\vec{r})=\vec{E}_0(\vec{r})e^{i\vec{k}\cdot\vec{r}}$, which substituted in Equation 14 gives:

$$\left\langle \vec{F} \right\rangle=\frac{1}{4}\mathrm{Re}\{\alpha(\omega)\}\nabla\left|\vec{E}_0\right|^2+\frac{1}{2}\vec{k}\,\mathrm{Im}\{\alpha(\omega)\}\left|\vec{E}_0\right|^2-\frac{1}{2}\mathrm{Im}\{\alpha(\omega)\}\mathrm{Im}\left\{\vec{E}_0\cdot\nabla\vec{E}_0^{*}\right\} \tag{15}$$

Equation 15 is the average force due to the radiation light field on the oscillator. The real part of the equation accounts for the dipole (or gradient) force, while the imaginary part is responsible for the absorption-plus-scattering longitudinal component of the force (loss/transfer of momentum from the incident light to the particle). Notice that the last term in 15 is zero when either $\vec{E}_0$ or α is real. This is the case for a propagating or evanescent plane

wave (but not for a beam in general) and for non-absorbing particles, respectively. The imaginary part of α is often assumed zero for dielectric, transparent particles—yet the approximation may not be valid, in general, for metallic particles,[15] as it will be discussed later.

Classical Approach

For small particles (Rayleigh regime) in an aqueous medium, the relative complex polarizability $\alpha(\omega)$ can be approximated as:[16]

$$\alpha(\omega) = \frac{\alpha_0(\omega)}{1-(2/3)ik^3\alpha_0(\omega)} \tag{16}$$

where $\alpha_0(\omega) = a^3(\varepsilon-1)/(\varepsilon+2)$ is the Clausius-Mosotti relation. The quantity $\varepsilon = \varepsilon_p/\varepsilon_m$ is the ratio of the (complex) permittivities of the particle and the surrounding medium, and a is the radius of the particle. The gradient force is obtained by substituting the real part of the polarizability $\alpha(\omega)$ from Equation 16 into 15:

$$\begin{aligned}\left\langle \vec{F}_{grad} \right\rangle &= 4\pi\varepsilon_m a^3 \left(\frac{\varepsilon-1}{\varepsilon+2}\right)\frac{1}{2}\nabla E_0^2 = \\ &= 4\pi m_m^2 \varepsilon_0 a^3 \left(\frac{m^2-1}{m^2+2}\right)\frac{1}{2}\nabla E_0^2 = \\ &= 4\pi m_m^2 \varepsilon_0 a^3 \left(\frac{m^2-1}{m^2+2}\right)\frac{1}{2}\nabla I(\vec{r})\end{aligned} \quad , \tag{17}$$

where the time average relations $\left\langle \vec{E}^2(\vec{r},t) \right\rangle = \tfrac{1}{2}\left|\vec{E}(\vec{r})\right|^2 = \tfrac{1}{2} I(\vec{r})$ are used. The last two equalities in Equation 17 have been written in the most common form—i.e. in terms of refractive indeces rather than permittivities—with $m = n_p/n_m$ being the relative refractive index, and n_p and n_m the refractive index of the particle and the medium, respectively. Note the dependence of the force with the gradient of the field intensity, which implies that the direction of the force for the induced dipole is towards the high-intensity regions of the beam.

Integrating Equation 17 highlights the fact that the dipole (gradient) force acts as it derives from a potential $\vec{F}_{grad}(\vec{r}) = -\nabla U_{grad}(\vec{r})$ where:

$$U_{grad}(\vec{r}) = 4\pi n_m^2 \varepsilon_0 a^3 \left(\frac{m^2 - 1}{m^2 + 2} \right) \frac{1}{2} I(\vec{r}) \tag{18}$$

In Equation 18, the integration constant is conventionally chosen to give a zero potential outside the light field of the beam.

In the classical framework, the absorption-plus-scattering longitudinal force is obtained by substituting the imaginary part of the polarizability $\alpha(\omega)$ from Equation 16 into 15. Under the Rayleigh approximation, the absorbing-plus-scattering force can be expressed in terms of the absorbing (σ_{abs}) and scattering (σ_{scatt}) cross section as:[17]

$$\vec{F}_{abs+scatt} = \frac{\left|\vec{E}_0\right|^2}{8\pi} (\sigma_{abs} + \sigma_{scatt}) \frac{\vec{k}}{k} \tag{19}$$

where $\vec{k}$ is the wave vector as per the usual convention, and where:[15]

$$\sigma = \sigma_{abs} + \sigma_{scatt} = 4\pi k a^3 \, \mathrm{Im}\left\{ \frac{\varepsilon - 1}{\varepsilon + 2} \right\} + \frac{8\pi}{3} k^4 a^6 \left| \frac{\varepsilon - 1}{\varepsilon + 2} \right|^2 \tag{20}$$

The first term in Equation 20 leads to the radiation pressure of the wave onto the particle due to absorption, whereas the second term leads to the scattering contribution of the force. In general, for transparent dielectric particles the absorption is considered negligible (i.e. $\sigma_{abs} \sim 0$) and the force in Equation 19 is determined almost solely by the scattering of the photons carrying momentum. The scattering force is the result of the difference between the momentum of the input beam (in the direction of propagation) and the secondary photons scattered by the induced oscillating dipole (in all directions):[18]

$$\left\langle \vec{F}_{scatt}(\vec{r}) \right\rangle = \frac{\sigma_{scatt} \left\langle \vec{S}_P(\vec{r}, t) \right\rangle}{c / n_m} = \hat{z} (n_m / c) \sigma_{scatt} I(\vec{r}), \tag{21}$$

where $\left\langle \vec{S}_P(\vec{r},t) \right\rangle$ is the time-averaged Poynting vector and $\hat{z}$ is the unit vector in the beam propagation direction. Substituting the second term of Equation 20 in Equation 21 produces the following—most familiar—expression of the scattering force for Rayleigh, transparent dielectric particles (written again for $m = n_p/n_m$ rather than ε):[18]

$$\left\langle \vec{F}_{scatt}(\vec{r}) \right\rangle = \hat{z}\frac{n_m}{c}\frac{8}{3}\pi(ka)^4 a^2\left(\frac{m^2-1}{m^2+2}\right)^2 I(\vec{r}) \tag{22}$$

Note how the scattering force points in the same direction the beam is propagating. It depends strongly on the wavelength ($\sim\lambda^{-4}$) and the intensity of the beam, as well as the size ($\sim a^6$) of the particle.

Gaussian beams. Equation 17 and 22 describe the gradient and scattering forces a small, transparent, dielectric particle is subject to due to interaction with the electromagnetic field. In both expressions, the actual field plays a central role in determining behaviour and motion of the particle in the optical trap. To this end, it is possible to derive the specific equations for F_{grad} and F_{scatt} in the case of a particle interacting with a Gaussian laser beam—one of the most conventional beam profile employed in optical traps (Figure 2b).[18] The dielectric sphere (radius a, refractive index n_p, dielectric permittivity ε_p) is considered suspended in a medium (refractive index n_m, dielectric permittivity ε_m, magnetic permeability μ_m) and illuminated by a linearly polarized Gaussian beam at the fundamental mode. The beam, with radius w_0 at its beam-waist position, is propagating along the z-axis and has its electric field parallel to the x-axis. Within the zeroth-order approximation in the paraxial Gaussian beam description, the electric field vector at the position $\vec{r} = (x, y, z)$ in terms of complex amplitude $\vec{E}(\vec{r},t)$ is:[18]

$$\vec{E}(\vec{r},t) = \hat{x}E(\vec{r}) = \hat{x}E_0\frac{ikw_0^2}{ikw_0^2+2z}e^{-ikz}e^{\left[-i\frac{2kz(x^2+y^2)}{(kw_0^2)^2+(2z)^2}\right]}e^{\left[-\frac{(kw_0)^2(x^2+y^2)}{(kw_0^2)^2+(2z)^2}\right]}e^{-i\omega t} \tag{23}$$

where $\hat{x}$ is the unit vector in the polarization direction, $k = n_m\omega/c$ is the wave number in the medium, and E_0 the electric field strength at the beam waist centre. The associated magnetic field vector is:[18]

$$\vec{H}(\vec{r},t) = \hat{z}\times\frac{\vec{E}(\vec{r},t)}{Z_0} \cong \hat{y}n_m\varepsilon_0 cE(\vec{r},t) = \hat{y}H(\vec{r},t), \tag{24}$$

where $Z_0 = \sqrt{\mu_m/\varepsilon_m} \cong 1/n_m\varepsilon_0 c$ is the intrinsic impedance of the medium for plane waves, $c = 1/\sqrt{\mu_0\varepsilon_0}$ is the speed of light in vacuum, and ε_0 and μ_0 the dielectric permittivity and magnetic permeability in vacuum, respectively. Note that the relationships $\varepsilon_m \cong \varepsilon_0 n_m^2$ and $\mu_m \cong \mu_0$, valid for a non-conducting and non-magnetic medium, are used in the above formulation. The Poynting vector, which describes the instantaneous energy flux crossing a unit area per unit time in the beam direction of propagation is:

$$\vec{S}_P(\vec{r},t) \equiv \vec{E}(\vec{r},t)\times\vec{H}(\vec{r},t). \tag{25}$$

Finally, the beam intensity, defined as the time average of the Poynting vector is:

$$\begin{aligned}\vec{I}(\vec{r}) \equiv \left\langle \vec{S}_P(\vec{r},t)\right\rangle &= \frac{1}{2}\mathrm{Re}\left[\vec{E}(\vec{r})\times\vec{H}^*(\vec{r})\right] = \\ &= \hat{z}\,\frac{n_m\varepsilon_0 c}{2}\left|E(\vec{r})\right|^2 = \tilde{z}I(\vec{r})\end{aligned}, \tag{26}$$

where:[18]

$$I(\vec{r}) = \left(\frac{2P}{\pi w_0^2}\right)\frac{1}{1+(2\tilde{z})^2}e^{\left[-\frac{2(\tilde{x}^2+\tilde{y}^2)}{1+(2\tilde{z})^2}\right]}. \tag{27}$$

The quantity $P = \pi\omega_0^2 n_m\varepsilon_0 cE_0^2/4$ is the beam power, while $\tilde{x}$, $\tilde{y}$ and $\tilde{z}$ are the normalized spatial coordinates given by $(\tilde{x},\tilde{y},\tilde{z}) = (x/\omega_0, y/\omega_0, z/k\omega_0^2)$.

Equation 27 gives a consistent relationship between the complex amplitude of the electric field and the intensity for a Gaussian laser beam with the harmonic dependence. However, Equations 23–27 are not always fully rigorous: while being quite accurate when $w_0 >> \lambda$, they require higher-order corrections when tightly focused laser beams are considered.[19, 20]

Combining Equation 27 with 17 yields the gradient force in terms of its three rectangular components.[18] Note the restoring action ($F_{grad} < 0$) towards the beam-waist centre for values of the relative refractive index $m > 1$, and the strong proportionality ($\sim a^3$) to the size of the particle:

$$\vec{F}_{grad,x}(\vec{r}) = -\hat{x}\,\frac{2\pi n_m a^3}{c}\left(\frac{m^2-1}{m^2+2}\right)\frac{4\tilde{x}/w_0}{1+(2\tilde{z})^2}\left(\frac{P}{\pi w_0^2}\right)\frac{1}{1+(2\tilde{z})^2}\,e^{\left[-\frac{2(\tilde{x}^2+\tilde{y}^2)}{1+(2\tilde{z})^2}\right]} \tag{28}$$

$$\vec{F}_{grad,y}(\vec{r}) = -\hat{y}\,\frac{2\pi n_m a^3}{c}\left(\frac{m^2-1}{m^2+2}\right)\frac{4\tilde{y}/w_0}{1+(2\tilde{z})^2}\left(\frac{P}{\pi w_0^2}\right)\frac{1}{1+(2\tilde{z})^2}\,e^{\left[-\frac{2(\tilde{x}^2+\tilde{y}^2)}{1+(2\tilde{z})^2}\right]} \tag{29}$$

$$\vec{F}_{grad,z}(\vec{r}) = -\hat{z}\,\frac{2\pi n_m a^3}{c}\left(\frac{m^2-1}{m^2+2}\right)\frac{8\tilde{z}/(kw_0^2)}{1+(2\tilde{z})^2}\left[1-\frac{2(\tilde{x}^2+\tilde{y}^2)}{1+(2\tilde{z})^2}\right]\left(\frac{2P}{\pi w_0^2}\right)\frac{1}{1+(2\tilde{z})^2}\,e^{\left[-\frac{2(\tilde{x}^2+\tilde{y}^2)}{1+(2\tilde{z})^2}\right]} \tag{30}$$

As per Equation 17 and 18, it is possible to integrate the dipole components of the force in the *x*- and *y*-axis (Equation 28 and 29) for a Gaussian beam and define the corresponding potential:

$$U_{grad} = \frac{2\pi n_m a^3}{c}\left(\frac{m^2-1}{m^2+2}\right)\frac{2P}{\pi w_0^2} \tag{31}$$

To achieve stable strapping the depth of this potential well must be larger than the average kinetic energy of the particle generated by Brownian motion ($\sim k_B T$).

Similarly, substituting Equation 27 for the beam intensity into Equation 22 gives the expression for the scattering force in terms of the intensity distribution of a Gaussian beam:

$$\vec{F}_{scatt}(\vec{r}) = \hat{z}\,\frac{n_m}{c}\frac{8}{3}\pi(ka)^4 a^2\left(\frac{m^2-1}{m^2+2}\right)^2\left(\frac{2P}{\pi w_0^2}\right)\frac{1}{1+(2\tilde{z})^2}\,e^{\left[-\frac{2(\tilde{x}^2+\tilde{y}^2)}{1+(2\tilde{z})^2}\right]} \tag{32}$$

Semi-classical Approach: Two-level Atoms

Beyond the classical approach, it is relevant to derive the radiation forces for the light field interacting with single atoms from a semi-classical standpoint. The motivation is twofold. The

first is practical. Optical trapping for a two-level system is readily understood (**Figure 3**). Under resonance conditions (the energy of the incident photons matches the difference between any two electronic levels of the absorber) the force originates from the conservation of momentum of the absorbed and emitted photons—this is the radiation force. Out of resonance, the electromagnetic field of the laser perturbs the energies of the initial (ground) and final (excited) states (ac Stark shift). The field induces short-lived virtual transitions and produces a transient change to the internal electronic energy of the material. The relative position between the dipole and the local light field thus becomes important and a force originates without photon absorption—this is the gradient force. The second motivation is historical. Worth the 1997 Physics Nobel Prize (C. Cohen-Tannoudji, W. D. Phillips and S. Chu), the investigation of light-atoms interactions led to the development of new fields of research ranging from atom cooling and trapping, to high-resolution spectroscopy and interferometry of ultracold atoms, as well as the study of Bose-Einstein condensates—worth itself the Physics Nobel Prize in 2001 (E. Cornell, C. Wieman and W. Ketterle).

In the semiclassical framework, the light is considered quasi-resonant with the transition between the initial $|i\rangle$ and final $|f\rangle$ states of the atom, i.e. ω is close to $\omega_0 = (E_f - E_i)/\hbar$, with E_f and E_i being the energy of the final and initial states, respectively. The atom is assumed to be a closed two-level system where the lower state $|i\rangle$ is stable (infinite lifetime), while the upper level $|f\rangle$ is unstable and decays with a radiative lifetime Γ^{-1} due to spontaneous emission, towards $|i\rangle$. Within this approximation, the steady-state polarizability for the atom—using the projection of the transition dipole moment along the direction of the electromagnetic field $\vec{p}_{if} \cdot \vec{n}_E$—is given by:[21]

$$\alpha(\omega) = \frac{(\vec{p}_{if} \cdot \vec{n}_E)^2}{\hbar} \frac{(\omega_0 - \omega + i\Gamma/2)}{(\omega_0 - \omega)^2 + i\Gamma^2/4 + \omega_R^2/2} \tag{33}$$

where $\omega_R = (\vec{p}_{if} \cdot \vec{n}_E)E_0 / \hbar$ is the Rabi frequency and E_0 the electric field strength. In this description, saturation must be taken into account as it can potentially limit the magnitude of the induced dipole $\vec{p}$ —yet, despite being nonlinear, it does not affect the monochromatic time dependence of the induced dipole allowing Equation 12 to be valid even for saturation. Substituting Equation 33 into 15 gives the following expression for the cycle-averaged force:

$$\langle F \rangle = \hbar \frac{\omega_R^2 / 2}{(\omega_0 - \omega)^2 + i\Gamma^2 / 4 + \omega_R^2 / 2} \left[(\omega - \omega_0) \frac{\nabla E_0}{E_0} + \frac{\Gamma}{2} \nabla \varphi \right] \tag{34}$$

where the complex amplitude of the electric field is expressed in term of the real amplitude E_0 and phase φ as $\underline{\vec{E}}(\vec{r}) = E_0(\vec{r}) e^{i\varphi(\vec{r})} \vec{n}_E$, with $\vec{n}_E$ being the unit vector in the direction of the polarization. Notice that φ can be written in terms of the local $\vec{k}$ vector as $\varphi = \vec{k} \cdot \vec{r}$, which gives $\nabla \varphi = \vec{k}$. Introducing the saturation parameter *s*:[21]

$$s = \frac{I}{I_{sat}} \frac{\Gamma^2 / 4}{(\omega_0 - \omega)^2 + \Gamma^2 / 4} \tag{35}$$

where the intensity I and saturation intensity I_{sat} are:

$$I = \frac{\varepsilon_0 c}{2} E_0^2, \tag{36}$$

$$I_{sat} = 4\pi\varepsilon_0 \frac{\hbar^2 c \Gamma^2}{16\pi (\vec{p}_{if} \cdot \vec{n}_E)^2} = \frac{\Gamma^2}{2\omega_R^2} I \tag{37}$$

Equation 34 for the cycle-averaged force becomes:

$$\langle F \rangle = \frac{s}{1+s} \hbar \left[(\omega - \omega_0) \frac{\nabla E_0}{E_0} + \frac{\Gamma}{2} \nabla \varphi \right] \tag{38}$$

Equation 38 was originally derived via a full quantum-mechanical approach;[22] here quantum mechanics is used only in Equation 33 for the atomic polarizability of a two-level atom. Equations 35–38 highlight a few interesting aspects about the nature of the forces. From 35, it follows that the maximum value of the saturation parameter *s* occurs for exact resonance, i.e.

$\omega = \omega_0$: the expression *s*/(1+*s*) approaches from below—and cannot exceed—the value of one, which in effect limits the maximum value of the force (saturated conditions).

In Equation 38, the first term is responsible for the gradient force, which is of dispersive nature (Figure 3a). For angular frequencies $\omega < \omega_0$ (red detuning) the gradient force is proportional to $-\nabla E_0$. The negative sign indicates that the atom is attracted towards regions of high light-field intensity. Conversely, for $\omega > \omega_0$ (blue detuning) the gradient force is proportional to ∇E_0 and the atom is repelled from the high-intensity region of the beam. The force vanishes all together at resonance, $\omega = \omega_0$. As per the classical case of a dielectric particle—Equation 17 and 18—the gradient force can be expressed as $\vec{F}_{grad}(\vec{r}) = -\nabla U_{grad}(\vec{r})$, with:

$$U_{grad}(\vec{r}) = \frac{\hbar(\omega-\omega_0)}{2}\ln\left[1+\frac{\omega_R^2(\vec{r})/2}{(\omega_0-\omega)^2+\Gamma^2/4}\right] = \\ = \frac{\hbar(\omega-\omega_0)}{2}\ln\left[1+s(\vec{r})\right] \tag{39}$$

where the dependence on the position for the saturation parameter $s(\vec{r})$ is expressed explicitly, and the relations 35 and 37 are used. Note that in 39, as per 18, the integration constant is chosen to give zero potential outside the trapping beam. Equation 39 for the specific case of a Gaussian beam yields:

$$U_{grad} = \frac{\hbar(\omega-\omega_0)}{2}\ln\left[1+\frac{1}{2}\frac{(\vec{p}_{if}\cdot\vec{n}_E)^2}{\hbar^2}\frac{4P}{\pi w_0^2 n_m \varepsilon_0 c}\frac{1}{(\omega-\omega_0)^2+\Gamma^2/4}\right] \tag{40}$$

which is the two-level atomic system potential, analogous to that of Equation 31 for the classical case of a small dielectric particle. Equation 39 and 40 highlight that an atom can be trapped at the focus of a laser beam if this is negatively detuned ($\omega < \omega_0$); the atom lays in a potential well of depth:

$$\Delta U_{grad} = \frac{\hbar(\omega_0-\omega)}{2}\ln(1+s_{\max}), \tag{41}$$

where s_{max} is the saturation maximum. The trap depth increases for increasing intensities of the beam, and atoms are trapped so long as their kinetic energy is less than the depth of the well. The potential well has a minimum in the *x*- and *y*- directions, as well as in the orthogonal direction *z* the beam propagates in. In *x* and *y*, the typical well width is ~w_0 while in *z* it is $\sim z_R = \pi\omega_0^2/\lambda$, z_R being the Rayleigh length. For practical purposes, it is rather challenging to realize potential wells able to trap atoms with temperatures much above a few hundreds of millikelvins, and trapping of atoms occurs in combinations with other methods such as Doppler cooling (see below) and magneto-optical trapping.[23] Optical forces are effectively employed to produce so-called optical lattices, where atoms are trapped in a periodic, 3D array of microtraps realized via a corresponding dipole potential of multiple standing waves.[24, 25]

The last term in Equation 38 is the scattering component of the force (Figure 3b) and far from saturation (i.e. $I << I_{sat}$) it can be approximated as:

$$\langle F_{scatt} \rangle = \hbar\vec{k}\frac{\Gamma}{2}\frac{I}{I_{sat}}\frac{\Gamma^2/4}{(\omega-\omega_0)^2+\Gamma^2/4} \tag{42}$$

where the relation $\vec{k} = \nabla\varphi$ is used. Equation 42 shows that the scattering force has its maximum value at the atomic resonant angular frequency $\omega = \omega_0$. The resonance is Lorentzian, and its width is of the same order of the atomic linewidth Γ—assuming *s* is not large compared to 1. This highlights the fact that for the force to be of significance, a laser beam with linewidth less than Γ is needed.

For reference, it is interesting to determine the conditions under which trapping of a single atom is efficient in the case of a non-uniform field such as that of a Gaussian beam. Optical trapping occurs when the gradient component of the force is high enough to overcome radiation pressure, which usually requires the laser's intensity to vary significantly over short

length scales (i.e. $|\nabla|$ is of the order of $\vec{k}$). In this case, $\left|\vec{F}_{scatt}\right| / \left|\vec{F}_{grad}\right| \approx \Gamma / |\omega_0 - \omega|$. This means that for low detuning ($|\omega_0 - \omega| << \Gamma$) the radiation component of the force dominates, whereas for high detuning ($|\omega_0 - \omega| >> \Gamma$) the gradient component does. However, if the detuning is too large the dipole (gradient) force becomes weak as it is too far off-resonance. As a result, the optimal trapping conditions are obtained for detuning $(\omega_0 - \omega) \approx \sqrt{(\omega_R^2 / 2) + (\Gamma^2 / 4)}$. Note that whilst the gradient force is conservative, the scattering force is dissipative, which means that is the latter to be normally exploited to cool (or, in principle, heat) the motion of the atom within the gradient force potential.

Atom cooling. The scattering force can be harnessed to cool atoms down to extremely low temperatures or, in other words, to bring them almost to rest. First proposed by Hänsch and Schawlow[26] in 1975 and demonstrated by Chu and collaborators[27] in 1985, atom cooling is an application of the Doppler effect.

Consider a closed two-level atom with non-zero velocity *v* and irradiated by counter propagating laser waves $\vec{k}_1$ and $\vec{k}_2$ (such that $\vec{k}_2 = -\vec{k}_1$) both of angular frequency $\omega < \omega_0$, i.e. slightly below resonance (**Figure 4a**). In this configuration, the opposed scattering forces do not directly cancel out. In fact for a moving atom, the changes in light intensity are so fast that the internal state never reaches steady-state equilibrium, hence the radiative force derives from the atom's instantaneous internal state and its motion. The radiation pressure $\vec{F}_i$ (with *i* = 1, 2) exerted by the waves is:[21]

$$\vec{F}_i = \hbar \vec{k}_i \frac{\Gamma}{2} s_i , \tag{43}$$

with:

$$s_i = \frac{I / I_{sat}}{1 + 4\left[(\delta \pm k_i v_z) / \Gamma\right]^2} \tag{44}$$

In Equation 44, $\delta = \omega - \omega_0$ is the resonance detuning (which is negative under the working hypothesis), $k_i = \left|\vec{k}_i\right|$, v_z is the component of the velocity in the *z* direction the wave is propagating to, and the plus (minus) sign at the denominator is for $\vec{k}_1$ ($\vec{k}_2$). The sum of $\vec{F}_1$ and $\vec{F}_2$ produces the resulting force along the *z*-axis:

$$F_z = \hbar k \frac{\Gamma}{2} \frac{I}{I_{sat}} \left[\frac{1}{1 + 4(\delta - k v_z)/\Gamma^2} - \frac{1}{1 + 4(\delta + k v_z)/\Gamma^2} \right], \tag{45}$$

which is always opposite in sign to the velocity (in the *z*-direction) of the atom.

The interpretation of Equation 45 is that—in the reference frame of the atom—the Doppler effect brings the wave opposed to the motion of the particle closer to resonance, resulting in the radiation pressure it exerts to dominate over that of the counter-propagating one. In a different—yet equivalent—picture, if the atom is travelling against the propagation direction of one of the laser beams, the frequency—in the atom's system of reference—is shifted towards higher values (blue shift). Conversely, an atom moving in the same direction of the beam experiences a shift towards lower frequencies (red shift). If the laser frequency is tuned slightly below the atom resonance transition, the atom predominantly absorbs a photon when moving towards the beam. This absorption process slows the atom down, owing to conservation of momentum. From the excited state, the atom then reemits its excitation energy with the spontaneous emission of a photon—which does not favour any particular direction. Thus, averaged over many absorption and emission cycles, the Doppler shift leads to an incremental force opposing the motion which results in the atom losing its velocity and effectively cooling down (Figure 4b).

A force opposing the velocity, and proportional to it, is a friction-type force. A linear expansion of Equation 45 near $v_z = 0$ produces:

$$F_z = -M\gamma v_z, \tag{46}$$

where:[21]

$$\gamma = \frac{8\hbar k^2}{M}\frac{I}{I_{sat}}\frac{(-\delta/\Gamma)}{(1+4\delta^2/\Gamma^2)^2} \tag{47}$$

is the friction coefficient ($\gamma > 0$ for negative detuning, i.e. $\delta < 0$), and M is the mass of the atom. Equation 46 leads to a differential equation whose solution is a damped exponential with time constant γ. Therefore by using three pairs of counter-propagating laser beams arranged along three orthogonal axes, the atom can be slowed down in all spatial directions (Figure 4c). The three components of its velocity are damped, i.e. $d\vec{v}/dt = -\gamma\vec{v}$. The friction coefficient is maximum for $\delta = \Gamma/2$, for which:

$$\gamma_{\max} = \frac{\hbar k^2}{M}\frac{I}{I_{sat}} \tag{48}$$

For instance, for alkali atoms $\hbar k^2/M$ ~10^4 s^{-1}, and for values of I/I_{sat} ~10^{-1} the damping time $1/\gamma_{\max}$ for the velocities is below one millisecond. It is as if the atom was moving into an extremely viscous medium, which brought to refer to this configuration as optical molasses.[27] The frictional force is negligible if $v >> -\delta/k$, called capture velocity (which is usually in the range 1–10 $m \cdot s^{-1}$). Thus, if an atom moves into an optical molasses with a residual velocity of up to a few metres per second, such velocity is quickly damped (over a few ms) and the atom is cooled.

1.3.2. Additional Forces (for Dielectric Particles)

The gradient force is the key component of an optical trap. It acts over the range of several hundreds of nm and provides the restoring action—linear with the displacement—which pulls the particle towards the centre of the optical trap. The Hookean nature of the gradient force and the fact that the particle has mass and is suspended in liquid lead to an equation of motion which is governed by elastic, inertial and viscous forces, and is given by the Langevin equation:

$$M\ddot{x} + \beta\dot{x} + \kappa x = \sqrt{2D}\zeta(t) \quad (49)$$

In equation 49, which is written for compactness for a single axis (x), the first term is the inertial force component for a particle of mass M. The second term is the velocity-dependent viscous damping force. The quantity $\beta = 6\pi a\eta$ is the Stokes drag constant for a particle of radius a moving in a fluid of viscosity η; β needs to be corrected according to Faxen's law, if the particle is in proximity to a surface.[28] The third term is the optical restoring force with κ being the so-called trap stiffness. The right-hand side of the equation represents the fluctuating force due to Brownian motion, where $D = k_B T / \beta$ is the Stokes-Einstein diffusion coefficient. The quantity $\zeta(t)$ is a stochastic Gaussian noise representing the effect of the collisions with the molecules of the fluid; it satisfies $\langle \zeta(t) \rangle = 0$ and $\langle \zeta(t)\zeta(t') \rangle = \delta(t - t')$, where the brackets indicate average with respect to the distribution of realizations and the δ-function indicates that the force at time t is assumed uncorrelated with that at any other time.

In the absence of damping (e.g. in vacuum), Equation 49 becomes that of an ideal oscillator with a resonant frequency $f_{res} = (1/2\pi)\sqrt{(\kappa / M)}$. When damping is taken into account, Equation 49 gives rise to a response—in frequency—equivalent to that of a single-pole, low-pass filter with a corner frequency $f_c = \kappa / 2\pi\beta$.

In typical applications (e.g. in biology) the stiffness κ of the tweezers is of the order of 5×10^{-5} $N\cdot m^{-1}$ while the mass of a 1-μm diameter particle is $\sim5\times10^{-16}$ kg. Hence the resonant frequency of an undamped optical trap is f_{res} ~50 kHz. For the same particle in water, β = 10^{-8} $N\cdot s\cdot m^{-1}$, which corresponds to a corner frequency f_c ~1 kHz. The fact that f_c is significantly lower than f_{res} indicates that the oscillations of a particle in an optical trap in liquid are in the overdamped regime. Note also that—beyond damping—the surrounding fluid provides cooling against the heating effects of the trapping laser beam(s). At room temperature, the damping fluid is also a source of thermal input given by the product

k_BT between the temperature T and the Boltzmann's constant k_B. The random incidence of the liquid molecules onto the trapped particle results in a fluctuating thermal force which—according to the theory of equipartition of energy—produces a mean-squared deviation in position along one axis $\langle x \rangle$ such that:[29]

$$\frac{1}{2}\kappa\langle x^2 \rangle = \frac{1}{2}k_BT \tag{50}$$

For typical values of temperature (300 K) and trap stiffness (5×10^{-5} N·m^{-1}), the root mean square deviation value in position is of the order of 10 nm. This is non-negligible in the interest of measuring molecular scale events, yet if compared to the relatively large trapping range of standard optical tweezers (~300 nm), it reveals that it is unlikely for a trapped particle to spontaneously diffuse away from the trap centre. In the harmonic potential approximation, the overdamped oscillations of a particle in the optical trap can be described analytically. From the equation of motion 49 the expected value of the density of the position of the trapped bead is given by a Lorentzian:[30]

$$\langle P(f) \rangle = \frac{1}{2\pi^2}\frac{k_BT/\beta}{(f_c^2 + f^2)} \tag{51}$$

where $P(f)$ is the power density at frequency f and $f_c = \kappa/2\pi\beta$ is the corner frequency determined from the best fit to the power spectrum.

1.4. Optical Torque

Light can also produce optical torque owing to three different mechanisms.[31] Light carrying spin and angular momentum can cause an object to either spin on its axis or orbit around a central point, respectively.[32] There is also a gradient-force type of torque which acts on non-spherical objects and tends to align them along the beam in preferential directions.

1.4.1. Gradient-Force Torque

The torque due to the gradient force acts on objects for which the associated polarizability tensor matrix (embodying the relative, directional shift in electron distribution and thus the associated dipole moment) is non-symmetrical with respect to the three spatial components. A typical case is that of a cylindrical particle in which the diagonal of the polarizability matrix has different values $\alpha_{\parallel}$ and $\alpha_{\perp}$ for the longitudinal (axial) and transversal (orthogonal) direction, respectively. Such an object—for instance with $\alpha_{\parallel} > \alpha_{\perp}$ —would experience a torque in response to a linearly-polarised radiation field and align with its long axis parallel to the polarization plane, at right angles to the direction of propagation of the beam. Note however, that a cylindrical object larger than the beam waist would align with its axis parallel to the propagation direction to maximize the interaction with the high-intensity region of the laser. The expression for the nanoscale torque is:[31]

$$\tau = (\alpha_{\perp} - \alpha_{\parallel})(E_y \tilde{x} - E_x \tilde{y})E_z \tag{52}$$

where E_x, E_y and E_z are the electric field components directed in the *x*-, *y*- and *z*-directions, while $\tilde{x}$ and $\tilde{y}$ are the normalized *x*- and *y*-unit vectors.

1.4.2. Spin-Angular- and Orbital-Angular-Momentum Torque

Optical Torque can arise from the transfer of orbital angular momentum (OAM) and spin angular momentum (SAM) from the trapping beam to the particle—analogously to the relationship between linear momentum and radiation force. For electromagnetic fields, the linear and angular momentum flux densities $\vec{J}$ and $\vec{\varsigma}$ are such that:

$$\vec{J} = \vec{r} \times \vec{\varsigma}\,, \tag{53}$$

where $\vec{r}$ is the position vector. The momentum flux density $\vec{\varsigma}$ is:

$$\vec{\varsigma} = \vec{S}_P / c = \vec{E} \times \vec{H} / c \tag{54}$$

where $\vec{S}_P$ is the Poynting vector and *c* is the speed of light. In 54 the coupled electric and magnetic field are a spin-1 system and, generally, the total angular momentum flux $\vec{J}$ has a spin ($\vec{S}$) and an orbital component ($\vec{L}$) associated with the polarization and the spatial structure of the field, respectively:

$$\vec{J} = \vec{L} + \vec{S} \tag{55}$$

SAM is strongly related to the polarisation state of light and can thus only arise for beams that are either fully or partially circularly polarized ($\left|\vec{S}\right| = \pm\hbar$ per photon for circularly polarized light, where the sign is given by the chirality) with the induced torque being reduced in case of beam scattering and reflection. This type of torque was first demonstrated experimentally[33] in 1936 and has more recently been shown to produce rotations of particles around their axis with extremely high rates.[34]

OAM is related to a tilt of the wavefront as per the case of a screw wavefront dislocation with $e^{il\varphi}$ azimuthal phase dependence (this is often referred to as an optical vortex with the pitch of the screw defining the topological charge *l*). The orbital angular momentum is given by $\left|\vec{L}\right| = l\hbar$ per photon.[35-37] Note that whilst the spin angular momentum is such that its value does not depend on the choice of axis, the orbital angular momentum does.[38] An important difference between spin and orbital angular momentum is the fact that SAM is given by the polarization of light (which is a local quantity), while OAM is caused by a helically wound phase front (which is a global quantity). This means that small particles such as atoms or small molecules do not feel OAM as they only respond locally with a small region of the field, unaffected by the global phase profile of the phase front.[39] Hence, orbital angular momentum cannot be transferred to single cold atoms, but rather to extended systems—e.g. Bose-Einstein condensates and microparticles.

The spin and orbital components cannot usually be separated in a trivial manner: they decouple in the paraxial approximation,[40, 41] while they transfer to one another in strongly focused beams.[42] It is however possible to write expressions for the spin and orbital components. The Cartesian components of the time-averaged spin angular momentum flux density $\vec{s}$ are:[42]

$$\begin{aligned} s_x &= \varepsilon_0 \,\mathrm{Im}\{E_y E_z^*\}/\omega \\ s_y &= \varepsilon_0 \,\mathrm{Im}\{E_x^* E_z\}/\omega \\ s_z &= \varepsilon_0 \,\mathrm{Im}\{E_x E_y^*\}/\omega \end{aligned} \tag{56}$$

Where E_x, E_y and E_z are the Cartesian components of $\vec{E}$. The analogous orbital components are:[42]

$$\begin{aligned} l_x &= \varepsilon_0 \,\mathrm{Im}\{E_y(\vec{r}\times\nabla)E_z^*\}/\omega \\ l_y &= \varepsilon_0 \,\mathrm{Im}\{E_x^*(\vec{r}\times\nabla)E_z\}/\omega \\ l_z &= \varepsilon_0 \,\mathrm{Im}\{E_x(\vec{r}\times\nabla)E_y^*\}/\omega \end{aligned} \tag{57}$$

The set of Equations 56 and 57 can be used to calculate the torque exerted on an object by paraxial beams.[43] Low-order Laguerre Gaussian (LG) beams are the most easily realised light fields with orbital angular momentum.[35] For optical trapping, torus-shaped LG beams are of particular interest as particles are confined within the torus by transverse gradient forces and experience the torque due to OAM—thus moving continuously around the torus.

2. Optical Trapping at the Nanoscale

The nature and specificities of the optical forces acting upon single atoms and (sub)micrometre-sized dielectric objects highlights an important aspect of optical trapping: light manipulation of nanoparticles in the size range ~1–100 nm is inefficient. On the one hand, laser cooling of single atoms rely on the near-resonant, narrow-line excitation of specific atomic transitions—which is in general incompatible with nanoparticles. On the other

hand, optical manipulation of micrometre-sized objects is dependent on the light-particle dipole interaction energy. This scales down with the volume of the object, becoming remarkably weak for particles in the nanoscale range. Moreover, the thermal motion of the object increases as the size of the nanoparticle decreases owing to a reduction in the viscous drag, thereby favouring escape from the trap. Attempts to either scale up trapping techniques optimized for single atoms or scale down those designed for microparticles have shown intrinsic limitations. Yet in recent years, several new methods for optical trapping of nanoscale objects have been developed, for this size regime is of great interest for many emerging nanotechnologies. Here, I review these methods highlighting their advantages and limitations, and discuss potential, future advancements in the field.

2.1. Plasmon-Based Forces

The idea of employing plasmonic excitations to enhance optical trapping follows two separate approaches. The first—direct enhancement—harnesses plasmons supported in trapped metal nanoparticles (MNPs) to increase their interaction with the field. The second—indirect enhancement—exploits instead plasmons in external nanostructures, e.g. nanoantennas, nanoholes, nanopillars, etc., to generate enhanced fields for the trapping of nanoobjects.

2.1.1. Direct Plasmon Enhancement

In the Rayleigh limit, the optical forces are determined by the dipolar polarizability of the particle (Equations 16–22 and 28–32). The dependence on the trapping wavelength, as well as the spatial distribution of the optical field are critical in determining whether a (sub)micrometre particle can be held, stably, in the optical trap—namely the gradient force has to overcome the competing absorption-plus-scattering force and Brownian motion. Standard optical tweezers can trap micrometre-sized dielectric beads with powers below ~1

mW, but tens of mW and up to W of laser powers are required to hold spheres in the 100-nm and 10-nm size range, respectively.[10]

In this respect, metal nanoparticles can offer several advantages owing to their plasmonic nature.[44] Far from plasmon resonances, the optical response of small MNPs is mainly the optical response of the free-electron plasma, which generally leads to the particles having large polarizabilities in the near-infrared. As a result at certain wavelengths, MNPs show trapping efficiencies which are manyfold higher than those of dielectric nanospheres. For instance, in their pioneering work on trapping of MNPs, Svoboda and Block demonstrated that—with a 1,064-nm laser—gold nanospheres were trapped seven times more efficiently than polystyrene spheres of the same size, owing to their seven-time higher polarizability at that wavelength.[45]

Trapping of MNPs can also benefit from strong localized surface plasmon (LSP) resonances. These are surface eigenmodes associated to collective excitations of conduction electrons induced by an incident electromagnetic field, and confined in volumes with linear dimensions much smaller than the incident wavelength (and typically with very high saturation intensities).[46] When the trapping laser is resonant with the LSPs of the metal nanoparticle, various optical cross-sections increase dramatically and the electromagnetic field near the particle's surface is enhanced. Specifically (Equation 15 and 16), at resonance the imaginary part of the polarizability dominates over the real part and the scattering force overcomes the gradient force, making stable trapping of MNPs unlikely. Similarly, if the wavelength of the trapping laser is shorter than the LSP resonant wavelength, the real part of the polarizability is negative and trapping is impossible. However, the gradient force increases significantly when the trap wavelength is longer than the plasmon resonance—in this case, stable trapping is achievable.[15] In fact, near-resonant laser excitation of MNPs plasmon resonances has allowed stable optical trapping of particles only tens of nm in size.[47-50]

In addition, the frequency of the plasmon resonances depends on shape and size, as well as material of the nanoparticles, which means that ad-hoc tuneability is feasible.[51, 52] For instance, metallic nanorods display a strong longitudinal-plasmon resonance along the main axis which is tuneable from the visible to the near-infrared spectral range via tailoring the aspect ratio and composition of the rods.[52-55] The non-sphericity of rod-like MNPs also confers the additional degree of control associated with optical torque,[48, 56-58] which allows for the rotation and alignment of the metal nanoobjects in the trap.

Stable trapping of metal nanoparticles has however a few limitations. It is, in general, hard to control. It is the result of a critical balance between wavelength and power of the trapping laser as well as geometry, material and size of the particle, which leads to the scaling of the trapping efficiency and the switching between the stable and unstable conditions to be non-trivial.[47, 53, 59] Arguably though, the main limitation associated to optical trapping of MNPs is heating (~hundreds of $^{o}C \cdot W^{-1}$) of both the particle and the surrounding environment due to strong light absorption under resonant illumination.[60] While this has led to the employment of optically-trapped MNPs as highly-localized, nanoscale heat transducers,[61-63] it strongly limits their use in biological applications where opticution—the optical damage of biological samples beyond viability—is inadmissible.[64-67]

2.1.2. Indirect Plasmon Enhancement

The trapping volume of conventional far-field optical tweezers is limited by diffraction: the trapping potential is ultimately bound to the focal spot size of the laser and the associated confinement of the light field. Since the 1990s inspired by the progress of near-field microscopy,[68-70] several methods exploiting near-fields have emerged with the goal of achieving manipulation of atoms and nanoparticles beyond the diffraction limit—and potentially with lower laser intensities. These include plasmonic optical tweezers (POTs), which make use of surface plasmon resonances supported by metallic nanostructures (**Figure**

5). These structures are engineered to efficiently couple to propagating light and concentrate it into highly localized (to size smaller than the optical wavelengths), intense optical fields known as hot spots[71]—where the confinement and depth of the trapping potential is dramatically increased (Figure 5a, b).

Note that there exist two types of surface plasmons depending on the geometry of the metal structure. Surface plasmon polaritons (SPPs) are propagating electromagnetic surface modes associated to collective oscillations of the free electrons in the metal, driven by the electromagnetic field. They are sustained at a flat metal-dielectric interface and are evanescent modes decaying exponentially away from the interface. They cannot be directly coupled to propagating light, requiring a way to compensate for the momentum mismatch—for instance by illuminating the metal film under total internal reflection through a glass prism of higher refractive index than the dielectric (Figure 5a, b). The efficient coupling to an SPP mode concentrates the light at the metal surface into an intense and confined surface wave with a much larger intensity density than the incident one. Conversely, localised surface plasmons (LSPs) are associated with bound electron plasmas in nanoareas or nanoobjects with dimensions much smaller than the incident wavelength. SPPs have a continuous dispersion relation and thus exist over a wide range of frequencies, whilst LSPs exist only over a limited frequency range due to the constraints imposed by their finite dimensions. Their resonance frequencies are determined by the size and shape of the particle, as well as the dielectric functions of both the metal and the surrounding media. LSPs can be directly coupled to propagating light.

Following various theoretical proposals advanced in the late 1990s,[72-74] a decade later, the first experimental demonstrations of plasmonic tweezers started to appear.[75-79] In 2008, Grigorenko et al. first showed that, by using conventional optical tweezers to scan a 200-nm polystyrene nanosphere across coupled pairs of gold nanodots, the resulting trapping efficiency was increased by almost an order of magnitude (Figure 5c).[80] Their approach

advanced POTs development via establishing two key aspects. The chosen geometry with arrays of nanodots allowed for precise control of the localized plasmon resonance frequencies (excited by light at normal incidence). It also resulted in the first subwavelength, three-dimensional plasmonic trap—which was an advancement compared to previous realizations limited to one dimension.[75-77] In 2009, Righini et al. proposed a new gap-antenna geometry of POTs (consisting of two 500-nm long gold wires separated by a 30-nm gap) and reported the trapping of living Escherichia coli bacteria.[81] This was promptly followed by the demonstration of trapping of 10-nm metal particles by means of analogous plasmonic dipole antennas.[82]

Almost at the same time, an alternative approach was proposed to further enhance POTs efficiencies: self-induced back-action (SIBA) plasmonic optical trapping (Figure 5d).[83] In this case, the (dielectric) particle itself alters the plasmonic resonance of the metallic structure which results in an enhanced trapping force. Juan et al. showed efficient trapping of 100-nm and 50-nm polystyrene spheres, with incident powers of just 0.7 mW and 1.9 mW, respectively. This is a substantial decrease in relative intensity for the trapping laser and it translates in a corresponding significant reduction (~one order of magnitude) in the local field intensity within the trap.

The typical setup for POTs is based on the Kretschmann configuration shown in Figure 5a. This basic layout can be adapted to realize a wide range of geometries and variants of plasmonic optical tweezers based on metal nanostructures, including: nanopillars,[84] pads,[78, 79] antennas,[80, 81] nanopyramids,[85] nanoholes,[83] nanoapertures[86] and even fractal structures.[87] Recently, there have been a few new advancements in plasmonic-based trapping methods[88]—namely POTs on chiral plasmonic nanostructures,[89-91] POTs with femtosecond-pulsed lasers[92-96] and resonant[97-99] POTs of polystyrene,[100] Au,[48, 51, 60] Ag[101] and CuCl[102] nanoparticles, as well as fluorophore-labeled antibodies.[103]

Note that beyond the *i)* desirable sub-diffraction trapping volume, and *ii)* significantly reduced laser trapping intensities (to achieve stable trapping, compared to conventional OTs), POTs are also extremely attractive owing to *iii)* their potential ability to be integrated with other conventional plasmonic-based applications, such as plasmon-enhanced photochemistry[104] and high-resolution biosensing of proteins.[105] Nevertheless, the main limitation of POTs—as per the case of direct plasmon enhancement discussed in the previous section—is heating of the plasmonic nanostructures. Designs based on integrating ad-hoc heat sinks with the optical nanostructures have been recently realised to mitigate the issue.[84]

2.2. Optical Binding Forces

Optical binding is the force which originates between dielectric objects when subject, simultaneously, to intense optical fields.[106] In 1989, Burns et al.[107] showed experimentally that optical binding could be used to create bound states between polystyrene spheres, and later proposed an extension of the basic mechanism to realize ordered, complex condensed-matter systems (e.g. of particles and molecules).[108] The derivation of the force for two objects can be obtained with a simple model. Similarly to the description used in section 1.3, the objects are treated as harmonic oscillators, responding resonantly to an incident field. Each oscillator reacts to the Lorentz forces independently and gives rise to scattered fields, which, in turn, produce mutual forces between the oscillators themselves (**Figure 6a**). These mutual forces are of two origins. The first one spurs from the induced dipole moment of one oscillator responding to the gradient of the scattered electric field of the other. The second force is magnetic and results from the Lorentz-force term involving the cross product of the time derivative of the oscillator's dipole moment and the scattered magnetic-flux density from the nearby oscillator. Both forces act on a range longer than standard van der Waals-type forces as, for both, the induced dipole moment stays constant for increasing distance. The static (time-averaged) part of the force leads to optical binding, where the relative phase shift

associated to the retardation between the oscillators determines the sign of the force—as different distances produce different possible phase shifts.

Following the formalism from Burns et al., the interaction energy between the oscillators can be approximated as:[107]

$$W = -\frac{1}{2}\alpha^2 E^2 k^2 \cos(kr)/r \tag{58}$$

Where $\vec{r}$ is the distance between the oscillators; E is the amplitude of the electric field for a plane wave of wave vector $\vec{k}$ and angular frequency ω, incident on the pair of oscillators at an angle between $\vec{k}$ and $\vec{r}$ assumed small in the approximation of Equation 58. The quantity $\alpha = e^2/M(\omega_0^2 - \omega^2)$ is the polarizability of the oscillators, which are considered light particles of mass M and charge e, harmonically bound with resonant angular frequency ω_0 to a heavy mass of opposite charge. From Equation 58, bound states occur at separations near multiple wavelengths and with depths in the potential well falling off inversely with the distance between oscillators. For the binding force to occur at temperature T, the interaction energy must be $W \geq k_B T$ (at the first equilibrium point, $kr \cong 2\pi$), requiring the polarizability to be $\alpha > \sqrt{4\pi k_B T / E^2 k^3}$.

Due to the relative phase shifts, particles in the appropriate experimental conditions arrange themselves at discrete separations, corresponding to minima of the binding potential. Stable spatial configurations between objects can be realised even with a simple (e.g. plane-wave illumination) homogeneous beam (along the beam axis) owing to the light momentum redistribution in the incident beam by the objects, mediated by the reciprocal interaction between objects due to the scattered light.

In 2002-2003 two groups[109, 110] demonstrated, independently, longitudinal optical binding of microbeads in water (Figure 6b). The trap consisted of two counterpropagating, weakly focused beams with displaced foci. The design was such that the gradient component of the

force would pull and hold the particles along the beam axis, while the opposing scattering forces (from radiation pressure) would push the particles to accumulate in the central region of the trap between the displaced foci of the two beams. Interestingly, instead of coagulating as one would intuitively expect, the microspheres self-organized themselves in precise equilibrium positions with spacing equal to several times the diameter of the particles (Figure 6c). Following these pioneering demonstrations, more complex assembly of nanoparticles in two[111, 112] and three[112, 113] dimensions have been recently realised (Figure 6d–f), validating the use of definitions such as *new ordered states of matter* and *optical crystals*. In recent years, traps based on optical binding have been developed to exploit size, shape and chirality of the nanoobjects,[114, 115] to realize a wide range of non-trivial mesostructures[116-118] (Figure 6e), often in combination with other approaches such as plasmonic structures[119] (Figure 6f) or light-assisted templated self-assembly.[120]

2.3. Other Forces

To overcome some of the limitations of optical manipulation at the nanoscale, in 2017 Juan et al.[121] proposed a new approach for optical trapping of dielectric nanoparticles containing elevated densities of extrinsic atom-like impurities. Rather than relying on the standard trapping mechanism for dielectric microbeads (cf. Equation 17)—which is inefficient for nanoscale particles due to the scaling with the volume—a relative low-power laser beam resonant to the dipole transitions of the hosted atom-like impurities is employed. In essence, the near-resonant forces (atom-trapping regime) acting on the large ensemble of atom-like impurities would allow for the manipulation of the whole host nanoparticle (potentially ~tens of nm in size and with laser powers below the biological damage threshold of ~10 mW/μm^2). Their proof-of-principle experiment showed that optical trapping (in a standard OT) of diamond nanoparticles (~150-nm in size) containing many (~10^3/particle) nitrogen-vacancy (NV) centres, displayed a change in efficiency (~10% after normalization) in the presence of a

second laser near-resonant with the zero phonon line (ZPL) of the emitters. Despite the modest effect, the study advances a few new key concepts. It potentially opens a new field as the method can be generalised to other systems and materials. As a matter of fact, NV centres in nanodiamonds are possibly not the best candidate due to the relatively low density of defects achievable per nanoparticle, as well as the low transition dipole moment, compared—for instance—to other diamond colour centres such as the silicon-vacancy (SiV)[122] and the germanium-vacancy (GeV)[123] centres. More interestingly, the resulting force is dispersive in nature (cf. Equation 38 and 39). This means that tuning the trapping laser below or above resonance would change the sign of the force—from repulsive for blue detuning to attractive for red detuning—allowing for an additional degree of freedom in the context of nanoscale optical manipulation. The experiment also led to some fundamental results. It showed that the new trapping mechanism worked owing to the phenomenon of superradiance acting amongst the atom-like emitters,[124] which is associated to a nonlinear increase of the total transition dipole moment—thus to an enhanced trapping efficiency. Superradiance was shown to take place amongst NV centres in nanodiamonds, at room temperature in a follow-up paper.[125]

3. Optical Tweezers Designs

In this section, I review the main existing designs of optical tweezers. I highlight advantages and limitations of each solution and present some of their most relevant applications.

3.1. Conventional Optical Tweezers

The first three-dimensional optical trap is the two-beam trap proposed and realized by Ashkin in 1970,[4] introduced in section 1.2 (Figure 1, inset, bottom). Probably the most common

design of conventional optical tweezers consists of a single beam tightly focused by a high numerical aperture objective, which serves the dual purpose of focusing the trapping laser and imaging the trapped object (**Figure 7a**).[3, 29] The sample—usually a suspension of particles in water—is contained in a microfluidic chamber and placed onto a stage. Depending on the configuration, the sample and/or the trapping beam can be moved relatively to one another by means of a piezo-driven stage or a steerable mirror, respectively. When a steering mirror is used, a lens relay system is employed to produce a collimated laser beam always centred at the back aperture of the objective for minimum loss of light.[126, 127]

3.1.1. Tracking Systems

Depending on their size, particles can be visualised with a camera either directly (particles' size ~μm) or using scattered light in dark-field microscopy (particles' size ~tens of nm). Accurate tracking of the particles within the trap is however achieved using devices such as a quadrant photodiode or a balance photodetector (Figure 7a).[128] With reference to section 1.3.2, a trapped particle in a focused Gaussian beam behaves—in first approximation—as an overdamped harmonic oscillator occupying the position of minimum energy at the centre of the trap (Equation 49). If perturbed, the object experiences a linear restoring force proportional, through the so-called trap stiffness κ, to the displacement. The trap stiffness is one of the key parameters of an optical trap and is determined using two main methods (other approaches are possible):[29] either by monitoring the mean-squared deviation in position of the particle within the trap (Equation 50), or by measuring the frequency response of the particle's motion (Equation 51). Irrespective of the method, the particle's behaviour is determined via back focal plane interference, i.e. via the interference between light diffracted by the particle and the undiffracted beam.[126] The interference pattern is imaged onto a quadrant photodiode using relay optics. The quadrant photodiode measures the lateral (X, Y)

position of the particle with respect to the normalized output voltage signals from the four quadrants (note that the axial (Z) position can be measured from the total intensity of the four quadrants):

$$X = \frac{(A+D)-(B+C)}{A+B+C+D}$$
$$Y = \frac{(A+B)-(C+D)}{A+B+C+D} \quad (59)$$

The differential voltage signals between quadrants, generated from the interference pattern of the sphere, are roughly proportional to the particle's displacement. This information is then used to determine the trap stiffness κ via estimating either the mean-squared deviation in position (based on Equation 50), or the value for the corner frequency $f_c = \kappa / 2\pi\beta$ ($\beta = 6\pi a\eta$ is the Stokes drag constant for a particle of radius a moving in a fluid of viscosity η), extracted from the power spectrum of the dynamics, which shows Lorentzian distribution (as per Equation 51).[29, 30, 129]

3.1.2. Force Clamping and Wrenching

Force or position clamps are a type of OT configuration in which position and stiffness of the trapped object are controlled dynamically. Specifically, feedback logic is employed to keep the position of the object in the trap constant, by measuring and varying the force acting upon it.[130-136] Force clamps exists in different geometries: single-, two-bead- and three-bead configuration.[137] They are commonly used for displacement measurements, often in combination with piezo-driven stages to facilitate the trap-to-sample relative positioning.[138-140] They have extensively been used in biology, to measure the forces involved in stretching[130] and unfolding of proteins,[141, 142] and in DNA/RNA polymerase action,[133, 134, 139, 140] as well as to characterize the motion of certain molecular motors[143, 144] such as myosin[145] and kinesin

(Figure 7b).[132, 146] Optical torque wrenches[147] are the rotational analogous of force clamps; they can be used to apply torque to trapped objects, for instance via controlling the polarization of the incident light.

3.1.3. Multiple-Particle Trapping

Certain applications require simultaneous trapping of multiple particles via a single beam. This can be achieved utilizing different approaches. One method is to deflect the beam very rapidly—for instance by means of an acousto-optic deflector[131]—between different trap positions.[127, 148, 149] The time between consecutive scans of the beam on the same spot has to be less than the time it takes for the particle to drift off. Albeit difficult this is possible as the viscous drag can keep the particle in place while the beam is servicing another trap spot. The diffusion coefficient of an object in liquid is given by the Einstein relation $D = k_B T / \beta$, corresponding to a root mean square diffusion distance $d = (2Dt)^{1/2}$, over the time *t*. For reference, a 1-μm object in water has a diffusion coefficient $D = 4 \cdot 10^{-13}$ $m^2 \cdot s^{-1}$, which gives a 5-nm shift in position over 25 μs; this limits the number of particles that can be manipulated at the same time (Figure 7c, d).[150]

A second, conceptually simpler, approach for multiple-particle trapping consists in dividing the laser in different beams.[148] The paths have different deflection optics: control is thus more complex, but the appealing aspect is that the trapped objects can be moved independently at the same time. A third method for simultaneous trapping of particles relies on holographic optical tweezers, discussed below.

3.2. Holographic Optical Tweezers

The natural extension to the method of laser division for multiple trapping is beam-shaping. This consists in using diffractive optical elements (DOEs)—either static or dynamic—at the pupil's image to convert a single laser into multiple beams and thus realize multiple optical traps at definite positions, simultaneously. Examples of dynamic diffractive elements are computer-generated holograms, with the corresponding optical tweezers generally referred to as holographic optical tweezers (HOTs). The majority of holographic optical trapping is achieved via spatial light modulators (SLMs)—computer-programmable, liquid-crystal-based devices which can shape the incident light field. The SLM is usually placed in a plane conjugate to the objective focal plane (Figure 7a), so that the complex field distribution in the trapping plane of the sample is the Fourier transform of that in the SLM plane.[151, 152] By modulating both the light amplitude and phase at the SLM, any optical field obeying the wave equation (and within the accessible field of view and range of spatial frequencies of the objective) can be generated inside the sample chamber, making HOTs extremely flexible. Typical SLMs tend to be phase-modulation-only devices[153, 154] as amplitude modulation translates in undesirable power losses,[155] (though phase-modulation often results in the formation of undesired ghost traps in the chamber).

In alternative strategies, the SLM is placed in the Fresnel rather than in the Fourier plane, which gives a few advantages—namely the suppression of undesired diffraction orders, faster switching capabilities due to lower computation requirements and the ability to generate multiple optical traps by using multiple holograms at the same time.[156]

High-performance SLMs allows the realization of complex 2D and 3D optical trap structures (Figure 7e, f)[151, 154, 157-160] and can be used to create colloidal crystal templates for trapping of up to a few hundreds of particles, simultaneously.[161, 162]

3.3. Plasmonic Optical Tweezers

I described plasmonic optical tweezers (POTs) in detail in section 2.1.2, in the context of indirect plasmon-enhanced forces.

4. Analytical Techniques

Optical tweezers can be effectively integrated with other techniques to characterize the properties of the trapped objects or the surrounding environment non-invasively, label-free and with high selectivity. This also means that objects can potentially be investigated and selected based on specific physicochemical characteristics: photoluminescence signal, spectroscopic signature and chirality, as well as electronic, plasmonic and nonlinear behaviour—to mention a few. Typical setups often consists of two beams, one for the trapping of the object and a second one for characterization purposes—yet single-beam configurations are possible if the wavelength is suitable both for trapping and analysis. The choice of the lasers might depend on factors such as reducing the risk of photodamage and opticution (crucial for instance for biospecimens), or maximizing absorption and excitation of the nanostructure to characterize.

4.1. Photonic Force Microscopy

Photonic force microscopy is an offshoot of optical trapping and is based on the idea of using a trapped object as the sensing element of a scanning-force microscope.[163, 164] A trapped particle's Brownian motion is affected by the interaction with the local environment. Hence by tracking (e.g. interferometrically) its three-dimensional trajectory and measuring the histogram of its positions, it is possible to derive the interaction potential and corresponding forces that act on the particle. The concept is not very different from that of an atomic force microscope (AFM); the advantage of a photonic force microscope (PFM) is the low stiffness

of the scanning probe, which results in higher deflections and thus better sensitivities. For reference, an AFM mechanical cantilever with a spring constant of 1–0.1 $N \cdot m^{-1}$ can routinely detect forces in the range ~10^{-10} N; a trapped particle (size 2 μm, trapping laser power 150 mW) with an axial spring constant of ~10^{-4}–10^{-5} $N \cdot m^{-1}$ can detect forces ~10^{-12}–10^{-13} N in aqueous media.[163]

The motion of a trapped object due to thermal fluctuations, in one dimension, is given by the overdamped Langevin equation (cf. §1.3.2, Equation 49). Once the trap stiffness has been determined and thus the PFM has been calibrated, the trapped object can be used to scan surfaces and structures by measuring how the motion of the object in the trap is affected by the probe-sample interaction.[163, 165] Care must be taken to account for noise artefacts which are known to occur.[166, 167]

The main advantages of photon force microscopy are the ability to image soft structure[164] (due to the aforementioned relatively low stiffness of the probe) with high sensitivities,[13] as well as the ability to map 3D volumetric structures with fast temporal resolutions (~tens of kHz).[168] The main limit of PFMs is the spatial resolution—intrinsically limited by the size of the probe (the trapped object can be ~hundreds of nm) and by thermal fluctuations. To improve the spatial resolution, non-spherical probes,[169-172] and even light-guiding nanostructures[173] have been proposed and utilised. Non-spherical probes also have the advantage to potentially provide angular information.[174, 175]

Optically trapped objects have also been proposed and used as probes for near-field scanning optical microscopy (NSOM), with relatively high sensitivity and yet no photo/thermal damage.[176]

4.2. Photoluminescence Spectroscopy

Photoluminescence spectroscopy is routinely integrated with OTs as it is a relatively simple optical method to measure fluorescence, electronic and structural properties of the trapped objects. Microphotoluminescence has, for instance, been used to identify different crystal phases in the trapped object[177] or map structural inhomogeneities along its entire span for selection before assembly into a device.[178] The optical response including strong nonlinearities[173, 179] and even the chirality[180] of certain nanomaterials can be readily investigated. The versatility of photoluminescent spectroscopy integrated with OTs, is proven by even more advanced applications. Geiselmann et al.[181] for instance, showed the possibility to optically manipulate a diamond nanoparticle and addressing/controlling the spin state of a single nitrogen-vacancy (NV) centre hosted in it, while in the trap—which is intriguing for applications in vectorial, high-resolution magnetometry based on single-spin manipulation. OT-based spectroscopy is also largely used in biology where current methods allow for characterization of single molecules.[182, 183]

4.3. Raman Spectroscopy and Surface-Enhanced Raman Scattering

Raman OTs, are tweezers coupled with a high resolution spectrometer for chemical and physical (Raman) analysis of the trapped object. Since its first inception[184] in 1984, Raman OTs have become an important analysis tool owing to their ability to overcome some of the primary limitations of standard Raman spectroscopy—lack of selectivity, required long acquisition times and signal contamination upon fixation to a substrate.[185] The main advantage of Laser trapping Raman spectroscopy (LTRS) is the ability to perform analysis on trapped objects individually and selectively,[186] in liquid or air (i.e. substrate-free), in situ and with time-resolved capabilities (for instance to measure the response to certain environmental changes[187, 188]—crucial in biological settings). While Raman OTs find applications in many

fields, for example for selection and sorting of nanomaterials,[180, 189-191] the fact that they offer non-invasive and label-free imaging make them particularly appealing for biomedicine.[192, 193]

In the context of Raman OTs, metal nanoparticles (MNPs) are particularly interesting. Owing to their localized surface plasmon (LSP) resonances—and associated local enhancement of the electromagnetic field near the surface—they are ideal candidate for surface-enhanced Raman scattering (SERS), which allows for molecular vibration spectroscopy with high sensitivity.[194, 195] In combination with optical trapping, they can thus be—in effect—mobile, subwavelength spectral probes for ultrasensitive, label-free identification of molecular species, in liquid.[195, 196] They have been successfully used, for instance, for detection of single DNA molecules[197] and of proteins attached to their surface.[198] Remarkably, SERS probes could potentially be integrated with photonic force microscopy,[199] making PFM even more compelling as a sensing technique.

5. Fields of Application

In the course of this review, I have already highlighted many of the applications where optical trapping has a strong presence. In this last section, I overview a few fields where nanoscale optical trapping has been particularly impactful or offers promising future perspectives.

5.1. Optical Assembly

Optical trapping naturally offers itself as a powerful tool for fabrication and assembly of micro- and nanostructures. Whilst the yields can be comparatively lower than those obtainable by other means (chemistry, physisorption, optical lithography, etc.), the key advantage of OTs

is their ability to selectively position the nanoobjects in specific arrangements, and with control relatively to other structures.

5.1.1. Spatially-Resolved Photochemistry

The intense illumination at their focus and the freedom to manipulate objects make optical tweezers an ideal tool for spatially-resolved, sub-wavelength photochemistry. Microsurgery is a prime example of it.[200] Pioneered in 1991,[201] the technique relies on a pair of lasers at different wavelengths. A first infrared laser—only weakly absorbed by biological tissues—is used for manipulating the biological object, while a second ultraviolet laser—which is instead readily absorbed—is used to drill holes, weld and cut. The applications are numerous and include: injection of substances into cells (hole-drilling), cell-fusion to combine genetic material (welding), and microdissecting (cutting, **Figure 8a**).[202-205]

Beyond life science, OT-photochemistry is used for micro-ablation[206] as well as fabrication of sub-wavelengths nanostructures. Remarkable examples include the realization of functional micromachines. These are produced by deflecting a laser beam along predetermined shapes in a resin: the beam induces photopolymerization of the resin, which transitions into a rigid glass-like material of the same shape defined by the laser's trajectory. Made in the form of rotors and cogwheels, these elements can then be actuated by a second trapping laser and even transfer momentum between one another (Figure 8b).[207] In a similar fashion, optical tweezers have also been used to fabricate patterned electronic and photonic structures (e.g. of molecular compounds not suitable for vacuum deposition) by laser-induced, localized chemical reactions of solutions containing reagents.[208]

OT-photochemistry is also advantageous for assembly of heterogeneous structures from nanoparts. For instance, a single laser beam can be used to trap individual nanoparticles in solution and subsequently fix them—with sub-wavelength accuracy—to the substrate or to

other structures. The fixation process can rely on different mechanisms: hydrophobic or van der Waals interactions between the nanoparticle and the substrate,[209] laser-induced adhesion (transient melting)[210] or laser-induced photo-polymerization.[211] Other techniques exploiting similar approaches include optical printing of nanostructures onto a substrate from colloidal nanoparticles,[212-214] and multi-photon polymerization of three-dimensional patterns (e.g. waveguides) in colloidal crystals.[215, 216] Working electronic devices have been fabricated from nanowires tweezed and fused together (Figure 8c)[217, 218] or fused onto other structures (Figure 8d).[219]

The assembly process in these cases is serial—one particle at a time—thus of relatively low throughput. This limitation has led to the development of parallel nanopatterning schemes which exploit OTs capable of trapping several nanoparticles at once—e.g. by means of holographic optical tweezers (HOTs, cf. §3.2). Both two- and three-dimensional quasi-crystalline structures made up of over one hundred silica microspheres have been assembled using HOTs and photo-polymerization of the suspension (Figure 7e, f).[160, 220] In an alternative realization, optical force stamping lithography (OFSL) has been used to create two-dimensional patterns of 82-nm Au and 80-nm Ag particles with ~45-nm spatial accuracy.[221] A spatial light modulator was used to simultaneously capture target nanoparticles in solution—tailored to be electrostatically repelled by the substrate—and fix them onto the substrate via van der Waals attraction, as the laser helped the nanoparticles overcome the electrostatic repulsion.

The ability to both create and assemble—from parts—micro- and nanometre-scale, functioning devices (mechanical, photonic and electronic) makes spatially-resolved photochemistry with OTs extremely attractive for fabricating hierarchically-structured materials and technologies, with advanced applications ranging from sensing to optomechanics and microfluidics.

5.1.2. Optical Actuation

Optical tweezers are also ideal candidates for the actuation of micro- and nanomachines, with prospects in medical diagnostic and therapeutics, as well as sensing and micro/ nanofabrication.

Impressive examples of their potential for dynamic assembling and actuation of micromachines includes the operation of micro-hydraulic pumps[222] and valves[223] from optically trapped particles (Figure 8e, f). In the case of the micro-hydraulic pumps,[222] a piezo-electric mirror was used to rapidly deflect (at frequencies higher than the associated time scales for Brownian diffusion) a trapping laser beam (cf. §3.1.3) and arrange microspheres in functional structures. In a first design, OTs were used to rotate in opposite directions two pairs of 3-μm silica microspheres (‘dumbells’) inside a 6-μm microfluidic pocket, displacing the fluid in the connected microchannel and creating a net flow (~1 $nl \cdot h^{-1}$). A variation of this scheme consisted in a peristaltic pump made of six microspheres (size 3-μm) optically trapped in a line and moved in a ‘snake-like’ fashion (Figure 8e) to act as a sinusoidal pump (operating at ~2 Hz). In more advanced configurations, individual microspheres (one 3-μm and five 0.64-μm silica microspheres) were assembled by the OTs and locked into position by photopolymerization to form an arm-like structure free to pivot on one end (Figure 8f). The trapping laser was then used to actuate the arm, either to block the flow of other particles inside a straight microchannel or to sort them with a three-way action in a T-like microfluidic junction (Figure 8f). The combination of the OTs with the photpolymerization process is an extremely powerful tool for the realization of complex structures made of colloidal microspheres fused together.[223]

Another advantage of micro- and nanomanipulation via optical tweezers is the control over rotational degrees of freedom. A linearly-polarized laser, for instance, can be used to angularly align an optically trapped birefringent micro-object in liquid, either with the slow

axis parallel or perpendicular to the vibration plane of the electric field (based on the retardation of the bi-refringence).[224, 225] This is crucial for the alignment of microcomponents in, for instance, micro-optical systems where microlenses and microprisms need to be positioned along an optical axis and aligned angularly. Beyond alignment, OTs with polarized light can be used to induce rotation in micro-gears. In an elegant experiment,[226] circularly polarized light was used to transfer optical angular momentum to a 1-μm birefringent calcite ($CaCO_3$) particle in an optical trap. The particle was then moved, by the trapping laser, close to a 10-μm, SiO_2 cog-like disk, and its optical torque transferred by the motion of the surrounding fluid to the cog. In alternative schemes rotational transport can also be achieved by shaping the wavefront of the trapping laser.[151] For instance, a spatial light modulator can be used to create an optical vortex and induce the rotation of colloidal particles around its outer circumference. This occurs owing to the transfer of angular momentum carried by the helical beam to the particle, and differs from that carried by circularly polarized light—which would cause an absorbing particle to spin on its own axis.[227] Controlled rotation of multiple microspheres has also been demonstrated using spiral interference patterns. These can be created by interfering a Laguerre-Gassian light beam and a plane wave, whilst changing the path length of the interferometer—which causes the trapped particles to rotate in a controlled fashion around the spiral's axis.[228]

5.2. Force and Displacement Measurements for Biology

Optical tweezers possess a set of specific features which makes them particularly attractive for life science studies.[28, 29] *i)* They are non-invasive and can operate at wavelengths (~0.8–1.1 μm) where light is poorly absorbed by living matter; *ii)* they can access size (~nm) and force (~pN) regimes which are relevant for processes taking place between and within biomolecules; *iii)* they can be combined with other sensing and analytical techniques allowing

for target-specific characterization (cf. §4); and *iv)* they allow for fast (~kHz) investigation of multiple systems (which is an advantage over, e.g., magnetic tweezers), in parallel, via time-sharing and multiple-trapping methods (cf. §3.1.3).

Some of the most remarkable biological studies involving optical tweezers were conducted in the 1990s and early 2000s, when OTs were first used to characterize the motion of single motor proteins including kinesin, myosin and dynein,[229-231] as well as the forces involved in receptors-ligands binding[232-234] and the physics of biopolymers.[130, 235, 236] Myosin, kinesin and dynein are linear motor proteins: they convert the energy of adenosine triphosphate (ATP) hydrolysis into mechanical work and move along polymer substrates: myosin along actin filaments in muscles and other cells, and kinesin and dynein on microtubules. Being responsible for muscle contraction, organelle transport, and cell and chromosomal division in living organisms, they have been subject of intense research over the last few decades. Yet, measuring their motion has always been challenging as it occurs at relatively small lengths (~nm) and fast time scales (≤ms). With high spatial resolution (~nm) and fast (~kHz) dynamics, optical tweezers have historically played a pivotal role in investigating the force and motion of motor proteins while, in turn, benefitting from having a test-bed for the developing new trapping designs.

In one of the first realizations, a focused laser beam was employed to trap a silica particle (size ~0.6 μm) attached to a kinesin molecule. The kinesin was then brought in touch with a fixed microtubule, and—by means of the trapping laser itself—its step size was measured, interferometrically, as it moved along the microtubule.[229] This type of OT is referred to as single-bead geometry (**Figure 9a**). A similar approach—albeit different in configuration (three-bead geometry)—was used to measure the force and displacement of myosin proteins interacting with a suspended actin filament, whose extremity were attached to two silica beads (size ~1 μm) held in two separate OTs, while the myosin was attached to a bead anchored to the substrate (Figure 9b).[230] From these first designs, several different strategies have been

developed, tailored to studying specific biological systems.[137] For instance, the two-bead configuration (Figure 9c) is used to measure the force and extension of a filament whose extremities are attached to two beads held in two OTs—one fixed, the other gradually pulled away. The single-, two- and three-bead geometries are so-called static configurations, as opposed to the dynamic ones that include force clamp, position clamp and dynamic force spectroscopy geometries. Force clamps operate by moving the trapping laser beam dynamically to maintain the force acting on the bead constant (Figure 9d). Position clamps operate by having a trapping beam monitoring the position of one bead, whereas the other bead (the motor) is moved using an acousto-optic deflector (AOD) to oppose the detected movements and maintain the bead-actin-bead assembly fixed at its initial position (Figure 9e).[230, 237] Dynamic force spectroscopy is used to measure the force of molecular bonds (Figure 9f). Their rupture forces are measured at different loading rates. Constant loading rates are applied by moving the trapped bead at constant velocity, or by clamping the position of the bead relative to the optical trap and constantly increasing the optical power.[238]

These schemes have been, and still are, successfully employed to study motion and forces at size (~nm) and force (~pN) regimes relevant for biology.[232-234] Variation on force clamp designs have been used to study individual translocation events during DNA-to-RNA transcription by means of the RNA polymerase (RNAP) enzyme. During transcription, the RNAP moves progressively along the DNA template (creating a complementary RNA) by discrete steps of subnanometre length. Ultra-stable optical trapping systems were thus developed to monitor the process with the required ångström-level resolution. The transcriptional elongation by single molecules of Escherichia coli RNAP was found to show discrete steps averaging (3.7 ± 0.6) Å (Figure 9g–i).[239] This is 20-fold smaller than the 8-nm kinesin step measured by the single-bead geometry discussed above (Figure 9a)[229]—and thus a testament to the potential of OTs for exploring biological systems down to the single-molecule level, at room temperature, in real time (Figure 9j–l)[183, 239-242]

As mentioned a few times in the course of this review, arguably the major obstacle to the widespread use of optical trapping in biology is damage due to light absorption and heating. Nevertheless the field is constantly evolving, with these challenges driving the development of new approaches and solutions (e.g. ad-hoc cooling systems[84] or fast light modulation).[183, 243]

5.3. Optomechanics

Optomechanics focuses on the interaction between electromagnetic radiation and mechanical systems by way of radiation pressure.[244] The field's agenda is vast, and is mainly driven by the goal of realizing systems (e.g. transducers) which—whilst macroscopic—can reach motions (thus sensitivities) close to the limits imposed by quantum mechanics of ground-state, zero-point-fluctuations and of the uncertainty relation.[245] Such systems would be able to detect very weak forces, leading to the development of a large variety of ultra-high-resolution sensing applications,[246-248] as well as offering a test-bed for investigating non-equilibrium thermodynamics[249, 250] and a multitude of fundamental quantum phenomena.[251-254] The main idea of optomechanics pivots around fabricating an optical cavity whose resonance frequency depends on the displacement of some mechanical oscillator—e.g. two facing mirrors, one movable, confining light between them. As the oscillator moves, its resonant frequency changes and so does the radiation pressure exerted onto the mechanical object—cooling down its motion ideally to its ground state. Since the first theoretical inceptions,[255] several optomechanical candidate systems have been investigated,[256] including optically-trapped nanoparticles levitating in a high-finesse optical cavity.[257] In fact, being physically detached from any other mechanical object, a levitating NP offers a low-noise, undamped environment, ideal for reaching ground-state cooling. One of the possible implementations consists in using a trapping laser (e.g. orientated vertically) to levitate a dielectric particle and a second driving

laser perpendicular to it (e.g. along a horizontal axis, *z*) and confined between two facing mirrors to form a high-finesse cavity, such that the radiation pressure of the driving field would cool down the mechanical motion to the ground state (**Figure 10a**). Alternative schemes include self-trapping using two optical modes combined to provide both trapping and optomechanical coupling,[257] and single-beam parametric feedback cooling schemes (Figure 10b).[258]

Optical levitation has been proposed and realized a few decades ago, yet at the time feedback cooling was beyond reach.[259, 260] The field has experienced a dramatic surge in interest in the last few years and recently optical levitation has improved to the point of enabling the measurement of zeptonewton forces[261] and radiation-pressure shot noise,[262] as well as the demonstration of centre-of-mass motion cooling of micron-sized (3 μm)[263] and nano-sized (~70 nm)[258] particles down to ~mK temperatures (Figure 10b)—with prospects for reaching even lower values (~μK).[264] These demonstrations hold great promise in the context of high-resolution detection and sensing[265] with force sensitivities potentially ~10^{-20} $N \cdot Hz^{-1/2}$ (i.e. orders of magnitude greater than most other force measurement techniques).[266] Realistic applications include detection of single electron or nuclear spins (Figure 10c–f),[267, 268] Casimir forces[269] and vacuum friction,[269, 270] phase transitions, and non-Newtonian gravity-like forces.[265]

6. Conclusions and Outlook

The field of optical trapping is incredibly active. Yet, while at opposite side of the spectrum OT techniques are well-established—ultracold atom physics on one side and manipulation of micron-sized particles on the other—optical manipulation of nanoscale objects is still developing. The limited success in either scaling up or down the techniques respectively

available for single atoms or microparticles, has exposed some of its inefficiencies, leaving quite a few barriers to overcome. These include the desirable need for: *i)* reducing the volume of the OTs for better specificity [sensing and characterization], *ii)* reaching sub-nanometre trapping accuracy [sensing and integrated nanofabrication], *iii)* achieving precise and repeatable manipulation of many (hundreds to thousands) nanoobjects, simultaneously [integrated nanofabrication], as well as *iv)* limiting invasive effects such as photodamage and heating [biomedical sensing and drug delivery].

With these challenges also come opportunities and what seems to be clear is that, in parallel with optimizing methods which already exist, new approaches will expectedly be advanced to progress the ever-growing field's agenda.

Acknowledgements

C.B. is funded by a University of Technology of Sydney Chancellor's Postdoctoral Research Fellowship and by an ARC Discovery Early Career Researcher Award (DE180100810).

Received: ((will be filled in by the editorial staff))
Revised: ((will be filled in by the editorial staff))
Published online: ((will be filled in by the editorial staff))

References

[1] J. H. Poynting, *Phil. Mag. (Presidential Address, Physical Society AGM, February 1905)*, **1905**, 9, 393-406.
[2] A. Ashkin, *Phys. Rev. Lett.*, **1970**, 24, 156-159.
[3] A. Ashkin, *IEEE Journal of Selected Topics in Quantum Electronics*, **2000**, 6, 841-856.
[4] A. Ashkin, *Phys. Rev. Lett.*, **1970**, 25, 1321-1324.
[5] S. Chu, *Reviews of Modern Physics*, **1998**, 70, 685-706.
[6] C. N. Cohen-Tannoudji, *Reviews of Modern Physics*, **1998**, 70, 707-719.
[7] W. D. Phillips, *Reviews of Modern Physics*, **1998**, 70, 721-741.
[8] I. Bloch, J. Dalibard, W. Zwerger, *Reviews of Modern Physics*, **2008**, 80, 885-964.
[9] S. Giorgini, L. P. Pitaevskii, S. Stringari, *Reviews of Modern Physics*, **2008**, 80, 1215-1274.
[10] A. Ashkin, J. M. Dziedzic, J. E. Bjorkholm, S. Chu, *Optics Letters*, **1986**, 11, 288-290.
[11] K. Dholakia, T. Cizmar, *Nat Photon*, **2011**, 5, 335-342.
[12] M. Padgett, R. Bowman, *Nat Photon*, **2011**, 5, 343-348.
[13] K. C. Neuman, A. Nagy, *Nature Methods*, **2008**, 5, 491-505.
[14] A. Ashkin, *Biophysical Journal*, **1992**, 61, 569-582.
[15] J. R. Arias-González, M. Nieto-Vesperinas, *J. Opt. Soc. Am. A*, **2003**, 20, 1201-1209.
[16] B. T. Draine, *Astrophysical Journal*, **1988**, 333, 848-872.
[17] P. C. Chaumet, M. Nieto-Vesperinas, *Optics Letters*, **2000**, 25, 1065-1067.
[18] Y. Harada, T. Asakura, *Optics Communications*, **1996**, 124, 529-541.
[19] L. W. Davis, *Physical Review A*, **1979**, 19, 1177-1179.
[20] J. P. Barton, D. R. Alexander, *J. Appl. Phys.*, **1989**, 66, 2800-2802.
[21] G. Grynberg, A. Aspect, C. Fabre, *Introduction to Quantum Optics: From the Semi-classical Approach to Quantized Light*, Cambridge University Press, Cambridge, **2010**.
[22] J. P. Gordon, A. Ashkin, *Physical Review A*, **1980**, 21, 1606-1617.
[23] S. Chu, *Science*, **1991**, 253, 861-866.
[24] P. Verkerk, B. Lounis, C. Salomon, C. Cohen-Tannoudji, J. Y. Courtois, G. Grynberg, *Phys. Rev. Lett.*, **1992**, 68, 3861-3864.
[25] P. S. Jessen, C. Gerz, P. D. Lett, W. D. Phillips, S. L. Rolston, R. J. C. Spreeuw, C. I. Westbrook, *Phys. Rev. Lett.*, **1992**, 69, 49-52.
[26] T. W. Hänsch, A. L. Schawlow, *Optics Communications*, **1975**, 13, 68-69.
[27] S. Chu, L. Hollberg, J. E. Bjorkholm, A. Cable, A. Ashkin, *Phys. Rev. Lett.*, **1985**, 55, 48-51.
[28] K. Svoboda, S. M. Block, *Annual Review of Biophysics and Biomolecular Structure*, **1994**, 23, 247-285.
[29] K. C. Neuman, S. M. Block, *Review of Scientific Instruments*, **2004**, 75, 2787-2809.
[30] K. Berg-Sørensen, H. Flyvbjerg, *Review of Scientific Instruments*, **2004**, 75, 594-612.
[31] D. S. Bradshaw, D. L. Andrews, *European Journal of Physics*, **2017**, 38, 034008.
[32] S. M. Barnett, L. Allen, R. P. Cameron, C. R. Gilson, M. J. Padgett, F. C. Speirits, A. M. Yao, *Journal of Optics*, **2016**, 18, 064004.
[33] R. A. Beth, *Physical Review*, **1936**, 50, 115-125.
[34] Y. Arita, M. Mazilu, K. Dholakia, *Nature Communications*, **2013**, 4, 2374.
[35] L. Allen, M. W. Beijersbergen, R. J. C. Spreeuw, J. P. Woerdman, *Physical Review A*, **1992**, 45, 8185-8189.
[36] J. Leach, M. J. Padgett, S. M. Barnett, S. Franke-Arnold, J. Courtial, *Phys. Rev. Lett.*, **2002**, 88, 257901.
[37] H. He, M. E. J. Friese, N. R. Heckenberg, H. Rubinsztein-Dunlop, *Phys. Rev. Lett.*, **1995**, 75, 826-829.
[38] A. T. O'Neil, I. MacVicar, L. Allen, M. J. Padgett, *Phys. Rev. Lett.*, **2002**, 88, 053601.
[39] M. Ritsch-Marte, *Optik & Photonik*, **2015**, 10, 32-37.

[40] M. V. Berry, *International Conference on Singular Optics*, **1998**, 3487, 6.
[41] S. M. Barnett, *Journal of Optics B: Quantum and Semiclassical Optics*, **2002**, 4, S7.
[42] T. A. Nieminen, A. B. Stilgoe, N. R. Heckenberg, H. Rubinsztein-Dunlop, *Journal of Optics A: Pure and Applied Optics*, **2008**, 10, 115005.
[43] S. J. Van Enk, G. Nienhuis, *Journal of Modern Optics*, **1994**, 41, 963-977.
[44] A. Lehmuskero, P. Johansson, H. Rubinsztein-Dunlop, L. Tong, M. Käll, *ACS Nano*, **2015**, 9, 3453-3469.
[45] K. Svoboda, S. M. Block, *Optics Letters*, **1994**, 19, 930-932.
[46] M. Pelton, M. Liu, S. Park, N. F. Scherer, P. Guyot-Sionnest, *Physical Review B*, **2006**, 73, 155419.
[47] P. M. Hansen, V. K. Bhatia, N. Harrit, L. Oddershede, *Nano Letters*, **2005**, 5, 1937-1942.
[48] M. Pelton, M. Liu, H. Y. Kim, G. Smith, P. Guyot-Sionnest, N. F. Scherer, *Optics Letters*, **2006**, 31, 2075-2077.
[49] L. Bosanac, T. Aabo, P. M. Bendix, L. B. Oddershede, *Nano Letters*, **2008**, 8, 1486-1491.
[50] F. Hajizadeh, S. N. S.Reihani, *Optics Express*, **2010**, 18, 551-559.
[51] K. C. Toussaint, M. Liu, M. Pelton, J. Pesic, M. J. Guffey, P. Guyot-Sionnest, N. F. Scherer, *Optics Express*, **2007**, 15, 12017-12029.
[52] C. Selhuber-Unkel, I. Zins, O. Schubert, C. Sönnichsen,L. B. Oddershede, *Nano Letters*, **2008**, 8, 2998-3003.
[53] E. Messina, E. Cavallaro, A. Cacciola, M. A. Iatì, P. G. Gucciardi, F. Borghese, P. Denti, R. Saija, G. Compagnini, M. Meneghetti, V. Amendola, O. M. Maragò, *ACS Nano*, **2011**, 5, 905-913.
[54] Z. Yan, J. E. Jureller, J. Sweet, M. J. Guffey, M. Pelton, N. F. Scherer, *Nano Letters*, **2012**, 12, 5155-5161.
[55] J. Pérez-Juste, I. Pastoriza-Santos, L. M. Liz-Marzán, P. Mulvaney, *Coordination Chemistry Reviews*, **2005**, 249, 1870-1901.
[56] M. Dienerowitz, M. Mazilu, P. J. Reece, T. F. Krauss, K. Dholakia, *Optics Express*, **2008**, 16, 4991-4999.
[57] P. H. Jones, F. Palmisano, F. Bonaccorso, P. G. Gucciardi, G. Calogero, A. C. Ferrari, O. M. Maragó, *ACS Nano*, **2009**, 3, 3077-3084.
[58] L. Tong, V. D. Miljković, M. Käll, *Nano Letters*, **2010**, 10, 268-273.
[59] R. Saija, P. Denti, F. Borghese, O. M. Maragò, M. A. Iatì, *Optics Express*, **2009**, 17, 10231-10241.
[60] Y. Seol, A. E. Carpenter, T. T. Perkins, *Optics Letters*, **2006**, 31, 2429-2431.
[61] G. Baffou, R. Quidant, *Laser & Photonics Reviews*, **2013**, 7, 171-187.
[62] L. Zuwei, H. Wei Hsuan, A. Mehmet, V. David, B. C. Stephen, *Nanotechnology*, **2010**, 21, 105304.
[63] P. M. Bendix, S. N. S. Reihani, L. B. Oddershede, *ACS Nano*, **2010**, 4, 2256-2262.
[64] K. C. Neuman, E. H. Chadd, G. F. Liou, K. Bergman, S. M. Block, *Biophysical Journal*, **1999**, 77, 2856-2863.
[65] A. Ashkin, J. Dziedzic, *Science*, **1987**, 235, 1517-1520.
[66] A. Ashkin, J. M. Dziedzic, T. Yamane, *Nature*, **1987**, 330, 769.
[67] A. Ashkin, J. M. Dziedzic, *Proceedings of the National Academy of Sciences*, **1989**, 86, 7914-7918.
[68] H. Heinzelmann, D. W. Pohl, *Applied Physics A*, **1994**, 59, 89-101.
[69] E. Betzig, J. K. Trautman, *Science*, **1992**, 257, 189-195.
[70] X. S. Xie, *Accounts of Chemical Research*, **1996**, 29, 598-606.
[71] V. M. Shalaev, A. K. Sarychev, *Physical Review B*, **1998**, 57, 13265-13288.
[72] O. J. F. Martin, C. Girard, *Appl. Phys. Lett.*, **1997**, 70, 705-707.

[73] L. Novotny, R. X. Bian, X. S. Xie, *Phys. Rev. Lett.*, **1997**, 79, 645-648.
[74] K. Okamoto, S. Kawata, *Phys. Rev. Lett.*, **1999**, 83, 4534-4537.
[75] V. Garcés-Chávez, R. Quidant, P. J. Reece, G. Badenes, L. Torner, K. Dholakia, *Physical Review B*, **2006**, 73, 085417.
[76] G. Volpe, R. Quidant, G. Badenes, D. Petrov, *Phys. Rev. Lett.*, **2006**, 96, 238101.
[77] P. J. Reece, V. Garcés-Chávez, K. Dholakia, *Appl. Phys. Lett.*, **2006**, 88, 221116.
[78] M. Righini, A. S. Zelenina, C. Girard, R. Quidant, *Nature Physics*, **2007**, 3, 477.
[79] M. Righini, G. Volpe, C. Girard, D. Petrov, R. Quidant, *Phys. Rev. Lett.*, **2008**, 100, 186804.
[80] A. N. Grigorenko, N. W. Roberts, M. R. Dickinson, Y. Zhang, *Nature Photonics*, **2008**, 2, 365.
[81] M. Righini, P. Ghenuche, S. Cherukulappurath, V. Myroshnychenko, F. J. García de Abajo, R. Quidant, *Nano Letters*, **2009**, 9, 3387-3391.
[82] W. Zhang, L. Huang, C. Santschi, O. J. F. Martin, *Nano Letters*, **2010**, 10, 1006-1011.
[83] M. L. Juan, R. Gordon, Y. Pang, F. Eftekhari, R. Quidant, *Nature Physics*, **2009**, 5, 915.
[84] K. Wang, E. Schonbrun, P. Steinvurzel, K. B. Crozier, *Nature Communications*, **2011**, 2, 469.
[85] Y. Tsuboi, T. Shoji, N. Kitamura, M. Takase, K. Murakoshi, Y. Mizumoto, H. Ishihara, *The Journal of Physical Chemistry Letters*, **2010**, 1, 2327-2333.
[86] Y. Pang, R. Gordon, *Nano Letters*, **2012**, 12, 402-406.
[87] G. Volpe, G. Volpe, R. Quidant, *Optics Express*, **2011**, 19, 3612-3618.
[88] T. Shoji, Y. Tsuboi, *The Journal of Physical Chemistry Letters*, **2014**, 5, 2957-2967.
[89] W.-Y. Tsai, J.-S. Huang, C.-B. Huang, *Nano Letters*, **2014**, 14, 547-552.
[90] W. Ma, H. Kuang, L. Xu, L. Ding, C. Xu, L. Wang, N. A. Kotov, *Nature Communications*, **2013**, 4, 2689.
[91] X. Wu, L. Xu, L. Liu, W. Ma, H. Yin, H. Kuang, L. Wang, C. Xu, N. A. Kotov, *Journal of the American Chemical Society*, **2013**, 135, 18629-18636.
[92] B. J. Roxworthy, K. C. Toussaint Jr, *Scientific Reports*, **2012**, 2, 660.
[93] Y. Jiang, T. Narushima, H. Okamoto, *Nature Physics*, **2010**, 6, 1005.
[94] J. C. Shane, M. Mazilu, W. M. Lee, K. Dholakia, *Optics Express*, **2010**, 18, 7554-7568.
[95] A. Usman, W.-Y. Chiang, H. Masuhara, *Journal of Photochemistry and Photobiology A: Chemistry*, **2012**, 234, 83-90.
[96] G. Bisker, D. Yelin, *Journal of the Optical Society of America B*, **2012**, 29, 1383-1393.
[97] T. Iida, H. Ishihara, *Phys. Rev. Lett.*, **2003**, 90, 057403.
[98] T. Iida, H. Ishihara, *Physical Review B*, **2008**, 77, 245319.
[99] T. Kudo, H. Ishihara, *Phys. Rev. Lett.*, **2012**, 109, 087402.
[100] M. A. Osborne, S. Balasubramanian, W. S. Furey, D. Klenerman, *The Journal of Physical Chemistry B*, **1998**, 102, 3160-3167.
[101] A. Ohlinger, S. Nedev, A. A. Lutich, J. Feldmann, *Nano Letters*, 2011, 11, 1770-1774.
[102] K. Inaba, K. Imaizumi, K. Katayama, M. Ichimiya, M. Ashida, T. Iida, H. Ishihara, T. Itoh, *physica status solidi (b)*, **2006**, 243, 3829-3833.
[103] H. Li, D. Zhou, H. Browne, D. Klenerman, *Journal of the American Chemical Society*, **2006**, 128, 5711-5717.
[104] K. Ueno, H. Misawa, *Journal of Photochemistry and Photobiology C: Photochemistry Reviews*, **2013**, 15, 31-52.
[105] M. Cottat, N. Thioune, A.-M. Gabudean, N. Lidgi-Guigui, M. Focsan, S. Astilean, M. Lamy de la Chapelle, *Plasmonics*, **2013**, 8, 699-704.
[106] K. Dholakia, P. Zemánek, *Reviews of Modern Physics*, **2010**, 82, 1767-1791.

[107] M. M. Burns, J.-M. Fournier, J. A. Golovchenko, *Phys. Rev. Lett.*, **1989**, 63, 1233-1236.
[108] M. M. Burns, J.-M. Fournier, J. A. Golovchenko, *Science*, **1990**, 249, 749-754.
[109] S. A. Tatarkova, A. E. Carruthers, K. Dholakia, *Phys. Rev. Lett.*, **2002**, 89, 283901.
[110] W. Singer, M. Frick, S. Bernet, M. Ritsch-Marte, *Journal of the Optical Society of America B*, **2003**, 20, 1568-1574.
[111] Z. Yan, R. A. Shah, G. Chado, S. K. Gray, M. Pelton, N. F. Scherer, *ACS Nano*, **2013**, 7, 1790-1802.
[112] Z. Yan, S. K. Gray, N. F. Scherer, *Nature Communications*, **2014**, 5, 3751.
[113] B. N. Slama-Eliau, G. Raithel, *Physical Review E*, **2011**, 83, 051406.
[114] D. S. Bradshaw, D. L. Andrews, *Physical Review A*, **2005**, 72, 033816.
[115] K. A. Forbes, D. L. Andrews, *Physical Review A*, **2015**, 91, 053824.
[116] S. H. Simpson, P. Zemánek, O. M. Maragò, P. H. Jones, S. Hanna, *Nano Letters*, **2017**, 17, 3485-3492.
[117] T. Kudo, S.-F. Wang, K.-i. Yuyama, H. Masuhara, *Nano Letters*, **2016**, 16, 3058-3062.
[118] S.-F. Wang, T. Kudo, K.-i. Yuyama, T. Sugiyama, H. Masuhara, *Langmuir*, **2016**, 32, 12488-12496.
[119] T. Shoji, M. Shibata, N. Kitamura, F. Nagasawa, M. Takase, K. Murakoshi, A. Nobuhiro, Y. Mizumoto, H. Ishihara, Y. Tsuboi, *The Journal of Physical Chemistry C*, **2013**, 117, 2500-2506.
[120] E. Jaquay, L. J. Martínez, C. A. Mejia, M. L. Povinelli, *Nano Letters*, **2013**, 13, 2290-2294.
[121] Mathieu L. Juan, C. Bradac, B. Besga, M. Johnsson, G. Brennen, G. Molina-Terriza, T. Volz, *Nature Physics*, **2016**, 13, 241.
[122] I. I. Vlasov, A. A. Shiryaev, T. Rendler, S. Steinert, S.-Y. Lee, D. Antonov, M. Voros, F. Jelezko, A. V. Fisenko, L. F. Semjonova, J. Biskupek, U. Kaiser, O. I. Lebedev, I. Sildos, P. R. Hemmer, V. I. Konov, A. Gali, J. Wrachtrup, *Nat Nano*, **2014**, 9, 54-58.
[123] T. Iwasaki, F. Ishibashi, Y. Miyamoto, Y. Doi, S. Kobayashi, T. Miyazaki, K. Tahara, K. D. Jahnke, L. J. Rogers, B. Naydenov, F. Jelezko, S. Yamasaki, S. Nagamachi, T. Inubushi, N. Mizuochi, M. Hatano, *Scientific Reports*, **2015**, 5, 12882.
[124] R. H. Dicke, *Physical Review*, **1954**, 93, 99-110.
[125] C. Bradac, M. T. Johnsson, M. v. Breugel, B. Q. Baragiola, R. Martin, M. L. Juan, G. K. Brennen, T. Volz, *Nature Communications*, **2017**, 8, 1205.
[126] W. M. Lee, P. J. Reece, R. F. Marchington, N. K. Metzger, K. Dholakia, *Nature Protocols*, **2007**, 2, 3226.
[127] E. Fällman, O. Axner, *Applied Optics*, **1997**, 36, 2107-2113.
[128] A. Pralle, M. Prummer, E. L. Florin, E. H. K. Stelzer, J. K. H. Hörber, *Microscopy Research and Technique*, **1999**, 44, 378-386.
[129] I. M. Tolić-Nørrelykke, K. Berg-Sørensen, H. Flyvbjerg, *Computer Physics Communications*, **2004**, 159, 225-240.
[130] M. D. Wang, H. Yin, R. Landick, J. Gelles, S. M. Block, *Biophysical Journal*, **1997**, 72, 1335-1346.
[131] K. Visscher, S. P. Gross, S. M. Block, *IEEE Journal of Selected Topics in Quantum Electronics*, **1996**, 2, 1066-1076.
[132] K. Visscher, M. J. Schnitzer, S. M. Block, *Nature*, **1999**, 400, 184.
[133] M. D. Wang, M. J. Schnitzer, H. Yin, R. Landick, J. Gelles, S. M. Block, *Science*, **1998**, 282, 902-907.
[134] G. J. L. Wuite, S. B. Smith, M. Young, D. Keller, C. Bustamante, *Nature*, **2000**, 404, 103.
[135] H. Ojala, A. Korsbäck, A. E. Wallin, E. Hæggström, *Appl. Phys. Lett.*, **2009**, 95, 181104.

[136] A. E. Wallin, H. Ojala, G. Ziedaite and E. Hæggström, *Review of Scientific Instruments*, **2011**, 82, 083102.
[137] M. Capitanio, Francesco S. Pavone, *Biophysical Journal*, **2013**, 105, 1293-1303.
[138] T. T. Perkins, H.-W. Li, R. V. Dalal, J. Gelles, S. M. Block, *Biophysical Journal*, **2004**, 86, 1640-1648.
[139] K. C. Neuman, E. A. Abbondanzieri, R. Landick, J. Gelles, S. M. Block, *Cell*, **2003**, 115, 437-447.
[140] K. Adelman, A. La Porta, T. J. Santangelo, J. T. Lis, J. W. Roberts, M. D. Wang, *Proceedings of the National Academy of Sciences*, **2002**, 99, 13538-13543.
[141] B. Jagannathan, S. Marqusee, *Biopolymers*, **2013**, 99, 860-869.
[142] J. Jiao, A. A. Rebane, L. Ma, Y. Zhang, in *Optical Tweezers: Methods and Protocols*, ed. A. Gennerich, Springer New York, New York, NY, **2017**, DOI: 10.1007/978-1-4939-6421-5_14, pp. 357-390.
[143] S. E. Rice, T. J. Purcell, J. A. Spudich, in *Methods in Enzymology*, Academic Press, **2003**, vol. 361, pp. 112-133.
[144] C. Veigel, C. F. Schmidt, *Nat Rev Mol Cell Biol*, **2011**, 12, 163-176.
[145] C. Batters, C. Veigel, in *Single Molecule Enzymology: Methods and Protocols*, eds. G. I. Mashanov, C. Batters, Humana Press, Totowa, NJ, **2011**, DOI: 10.1007/978-1-61779-261-8_7, pp. 97-109.
[146] S. M. Block, C. L. Asbury, J. W. Shaevitz, M. J. Lang, *Proceedings of the National Academy of Sciences*, **2003**, 100, 2351-2356.
[147] A. La Porta, M. D. Wang, *Phys. Rev. Lett.*, **2004**, 92, 190801.
[148] K. Visscher, G. J. Brakenhoff, J. J. Krol, *Cytometry*, **1993**, 14, 105-114.
[149] K. Sasaki, M. Koshioka, H. Misawa, N. Kitamura, H. Masuhara, *Optics Letters*, **1991**, 16, 1463-1465.
[150] C. Mio, T. Gong, A. Terray, D. W. M. Marr, *Fluid Phase Equilibria*, **2001**, 185, 157-163.
[151] J. E. Curtis, B. A. Koss, D. G. Grier, *Optics Communications*, **2002**, 207, 169-175.
[152] E. Martín-Badosa, M. Montes-Usategui, A. Carnicer, J. Andilla, E. Pleguezuelos, I. Juvells, *Journal of Optics A: Pure and Applied Optics*, **2007**, 9, S267.
[153] M. Reicherter, T. Haist, E. U. Wagemann, H. J. Tiziani, *Optics Letters*, **1999**, 24, 608-610.
[154] J. Liesener, M. Reicherter, T. Haist, H. J. Tiziani, *Optics Communications*, **2000**, 185, 77-82.
[155] E. G. van Putten, I. M. Vellekoop, A. P. Mosk, *Applied Optics*, **2008**, 47, 2076-2081.
[156] A. Jesacher, S. Fürhapter, S. Bernet, M. Ritsch-Marte, *Optics Express*, **2004**, 12, 2243-2250.
[157] D. G. Grier, *Nature*, **2003**, 424, 810.
[158] V. Bingelyte, J. Leach, J. Courtial, M. J. Padgett, *Appl. Phys. Lett.*, **2003**, 82, 829-831.
[159] D. G. Grier, Y. Roichman, *Applied Optics*, **2006**, 45, 880-887.
[160] Y. Roichman, D. G. Grier, *Optics Express*, **2005**, 13, 5434-5439.
[161] J. Leach, G. Sinclair, P. Jordan, J. Courtial, M. J. Padgett, J. Cooper, Z. J. Laczik, *Optics Express*, **2004**, 12, 220-226.
[162] P. T. Korda, D. G. Grier, *The Journal of Chemical Physics*, **2001**, 114, 7570-7573.
[163] L. P. Ghislain, W. W. Webb, *Optics Letters*, **1993**, 18, 1678-1680.
[164] A. Rohrbach, C. Tischer, D. Neumayer, E.-L. Florin, E. H. K. Stelzer, *Review of Scientific Instruments*, **2004**, 75, 2197-2210.
[165] E.-L. Florin, A. Pralle, J. K. Heinrich Hörber, E. H. K. Stelzer, *Journal of Structural Biology*, **1997**, 119, 202-211.
[166] G. Volpe, L. Helden, T. Brettschneider, J. Wehr, C. Bechinger, *Phys. Rev. Lett.*, **2010**, 104, 170602.

[167] T. Brettschneider, G. Volpe, L. Helden, J. Wehr, C. Bechinger, *Physical Review E*, **2011**, 83, 041113.
[168] C. Tischer, S. Altmann, S. Fišinger, J. K. H. Hörber, E. H. K. Stelzer, E.-L. Florin, *Appl. Phys. Lett.*, **2001**, 79, 3878-3880.
[169] M. R. Pollard, S. W. Botchway, B. Chichkov, E. Freeman, R. N. J. Halsall, D. W. K. Jenkins, I. Loader, A. Ovsianikov, A. W. Parker, R. Stevens, R. Turchetta, A. D. Ward, M. Towrie, *New Journal of Physics*, **2010**, 12, 113056.
[170] D. B. Phillips, D. A. Simpson, J. A. Grieve, R. Bowman, B. C. Gibson, M. J. Padgett, J. G. Rarity, S. Hanna, J. P. Miles, D. M. Carberry, *EPL (Europhysics Letters)*, **2012**, 99, 58004.
[171] S. N. Olof, J. A. Grieve, D. B. Phillips, H. Rosenkranz, M. L. Yallop, M. J. Miles, A. J. Patil, S. Mann, D. M. Carberry, *Nano Letters*, **2012**, 12, 6018-6023.
[172] D. B. Phillips, G. M. Gibson, R. Bowman, M. J. Padgett, S. Hanna, D. M. Carberry, M. J. Miles, S. H. Simpson, *Optics Express*, **2012**, 20, 29679-29693.
[173] Y. Nakayama, P. J. Pauzauskie, A. Radenovic, R. M. Onorato, R. J. Saykally, J. Liphardt, P. Yang, *Nature*, **2007**, 447, 1098.
[174] H. Kress, E. H. K. Stelzer, A. Rohrbach, *Appl. Phys. Lett.*, **2004**, 84, 4271-4273.
[175] O. M. Maragò, P. H. Jones, F. Bonaccorso, V. Scardaci, P. G. Gucciardi, A. G. Rozhin, A. C. Ferrari, *Nano Letters*, **2008**, 8, 3211-3216.
[176] K. Sasaki, H. Fujiwara, H. Masuhara, *Journal of Vacuum Science & Technology B: Microelectronics and Nanometer Structures Processing, Measurement, and Phenomena*, **1997**, 15, 2786-2790.
[177] P. J. Reece, S. Paiman, O. Abdul-Nabi, Q. Gao, M. Gal, H. H. Tan, C. Jagadish, *Appl. Phys. Lett.*, **2009**, 95, 101109.
[178] F. Wang, W. J. Toe, W. M. Lee, D. McGloin, Q. Gao, H. H. Tan, C. Jagadish, P. J. Reece, *Nano Letters*, **2013**, 13, 1185-1191.
[179] F. Wang, P. J. Reece, S. Paiman, Q. Gao, H. H. Tan, C. Jagadish, *Nano Letters*, **2011**, 11, 4149-4153.
[180] T. Rodgers, S. Shoji, Z. Sekkat, S. Kawata, *Phys. Rev. Lett.*, **2008**, 101, 127402.
[181] M. Geiselmann, M. L. Juan, J. Renger, J. M. Say, L. J. Brown, F. J. G. de Abajo, F. Koppens, R. Quidant, *Nat Nano*, **2013**, 8, 175-179.
[182] M. J. Lang, P. M. Fordyce, A. M. Engh, K. C. Neuman, S. M. Block, *Nature Methods*, **2004**, 1, 133.
[183] M. J. Comstock, T. Ha, Y. R. Chemla, *Nature Methods*, **2011**, 8, 335.
[184] R. Thurn, W. Kiefer, *Applied Spectroscopy*, **1984**, 38, 78-83.
[185] J. W. Chan, *Journal of Biophotonics*, **2013**, 6, 36-48.
[186] D. Fu, J. Zhou, W. S. Zhu, P. W. Manley, Y. K. Wang, T. Hood, A. Wylie, X. S. Xie, *Nature Chemistry*, **2014**, 6, 614.
[187] C. Xie, Y.-q. Li, W. Tang, R. J. Newton, *J. Appl. Phys.*, 2003, 94, 6138-6142.
[188] T. J. Moritz, D. S. Taylor, D. M. Krol, J. Fritch, J. W. Chan, *Biomed. Opt. Express*, **2010**, 1, 1138-1147.
[189] K. Ajito, K. Torimitsu, *Applied Spectroscopy*, **2002**, 56, 541-544.
[190] A. C. Ferrari, J. C. Meyer, V. Scardaci, C. Casiraghi, M. Lazzeri, F. Mauri, S. Piscanec, D. Jiang, K. S. Novoselov, S. Roth, A. K. Geim, *Phys. Rev. Lett.*, **2006**, 97, 187401.
[191] A. C. Ferrari, D. M. Basko, *Nature Nanotechnology*, **2013**, 8, 235.
[192] C. Xie, M. A. Dinno, Y.-q. Li, *Optics Letters*, **2002**, 27, 249-251.
[193] R. D. Snook, T. J. Harvey, E. Correia Faria, P. Gardner, *Integrative Biology*, **2009**, 1, 43-52.
[194] M. Moskovits, *Reviews of Modern Physics*, **1985**, 57, 783-826.

[195] K. Kneipp, H. Kneipp, I. Itzkan, R. R. Dasari, M. S. Feld, *Chemical Reviews*, **1999**, 99, 2957-2976.
[196] J. Prikulis, F. Svedberg, M. Käll, J. Enger, K. Ramser, M. Goksör, D. Hanstorp, *Nano Letters*, **2004**, 4, 115-118.
[197] S. Rao, S. Raj, S. Balint, C. B. Fons, S. Campoy, M. Llagostera, D. Petrov, *Appl. Phys. Lett.*, **2010**, 96, 213701.
[198] E. Messina, E. Cavallaro, A. Cacciola, R. Saija, F. Borghese, P. Denti, B. Fazio, C. D'Andrea, P. G. Gucciardi, M. A. Iatì, M. Meneghetti, G. Compagnini, V. Amendola, O. M. Maragò, *The Journal of Physical Chemistry C*, **2011**, 115, 5115-5122.
[199] Š. Bálint, M. P. Kreuzer, S. Rao, G. Badenes, P. Miškovský, D. Petrov, *The Journal of Physical Chemistry C*, **2009**, 113, 17724-17729.
[200] K. O. Greulich, *Rep. Prog. Phys.*, **2017**, 80, 026601.
[201] S. Seeger, S. Monajembashi, K. J. Hutter, G. Futterman, J. Wolfrum, K. O. Greulich, *Cytometry*, **1991**, 12, 497-504.
[202] H. Liang, W. H. Wright, S. Cheng, W. He, M. W. Berns, *Experimental Cell Research*, **1993**, 204, 110-120.
[203] K. Schüze, A. Clement-Sengewald, *Nature*, **1994**, 368, 667.
[204] M. W. Berns, in *Methods in Cell Biology*, Academic Press, **2007**, vol. 82, pp. 1-58.
[205] K. O. Greulich, in *Methods in Cell Biology*, Academic Press, **2007**, vol. 82, pp. 59-80.
[206] G. Fuhr, C. Reichle, T. Müller, K. Kahlke, K. Schütze, M. Stuke, *Applied Physics A*, **1999**, 69, 611-616.
[207] P. Galajda, P. Ormos, *Appl. Phys. Lett.*, **2001**, 78, 249-251.
[208] A. Lachish-Zalait, D. Zbaida, E. Klein, M. Elbaum, *Advanced Functional Materials*, **2001**, 11, 218-223.
[209] M. J. Guffey, N. F. Scherer, *Nano Letters*, **2010**, 10, 4302-4308.
[210] S. Ito, H. Yoshikawa, H. Masuhara, *Appl. Phys. Lett.*, **2002**, 80, 482-484.
[211] S. Ito, H. Yoshikawa, H. Masuhara, *Appl. Phys. Lett.*, **2001**, 78, 2566-2568.
[212] J. Gargiulo, I. L. Violi, S. Cerrota, L. Chvátal, E. Cortés, E. M. Perassi, F. Diaz, P. Zemánek, F. D. Stefani, *ACS Nano*, **2017**, 11, 9678-9688.
[213] J. Gargiulo, T. Brick, I. L. Violi, F. C. Herrera, T. Shibanuma, P. Albella, F. G. Requejo, E. Cortés, S. A. Maier, F. D. Stefani, *Nano Letters*, **2017**, 17, 5747-5755.
[214] M. A. Huergo, C. M. Maier, M. F. Castez, C. Vericat, S. Nedev, R. C. Salvarezza, A. S. Urban, J. Feldmann, *ACS Nano*, **2016**, 10, 3614-3621.
[215] T. A. Taton, D. J. Norris, *Nature*, **2002**, 416, 685.
[216] W. Lee, S. A. Pruzinsky, P. V. Braun, *Advanced Materials*, **2002**, 14, 271-274.
[217] P. J. Pauzauskie, A. Radenovic, E. Trepagnier, H. Shroff, P. Yang, J. Liphardt, *Nature Materials*, **2006**, 5, 97.
[218] R. Agarwal, K. Ladavac, Y. Roichman, G. Yu, C. M. Lieber, D. G. Grier, *Optics Express*, **2005**, 13, 8906-8912.
[219] S.-W. Lee, G. Jo, T. Lee, Y.-G. Lee, *Optics Express*, **2009**, 17, 17491-17501.
[220] J. Li, G. Du, *Applied Optics*, **2014**, 53, 351-355.
[221] S. Nedev, A. S. Urban, A. A. Lutich, J. Feldmann, *Nano Letters*, **2011**, 11, 5066-5070.
[222] A. Terray, J. Oakey, D. W. M. Marr, *Science*, **2002**, 296, 1841-1844.
[223] A. Terray, J. Oakey, D. W. M. Marr, *Appl. Phys. Lett.*, **2002**, 81, 1555-1557.
[224] E. Higurashi, R. Sawada, T. Ito, *Physical Review E*, **1999**, 59, 3676-3681.
[225] E. Higurashi, R. Sawada, T. Ito, *Journal of Micromechanics and Microengineering*, **2001**, 11, 140.
[226] M. E. J. Friese, H. Rubinsztein-Dunlop, J. Gold, P. Hagberg, D. Hanstorp, *Appl. Phys. Lett.*, **2001**, 78, 547-549.
[227] J. E. Curtis, D. G. Grier, *Phys. Rev. Lett.*, **2003**, 90, 133901.

[228] L. Paterson, M. P. MacDonald, J. Arlt, W. Sibbett, P. E. Bryant, K. Dholakia, *Science*, **2001**, 292, 912-914.
[229] K. Svoboda, C. F. Schmidt, B. J. Schnapp, S. M. Block, *Nature*, **1993**, 365, 721.
[230] J. T. Finer, R. M. Simmons, J. A. Spudich, *Nature*, **1994**, 368, 113.
[231] H. Sakakibara, H. Kojima, Y. Sakai, E. Katayama, K. Oiwa, *Nature*, **1999**, 400, 586.
[232] H. Miyata, R. Yasuda, K. Kinosita, *Biochimica et Biophysica Acta (BBA) - General Subjects*, **1996**, 1290, 83-88.
[233] K. Kawaguchi, S. i. Ishiwata, *Science*, **2001**, 291, 667-669.
[234] T. Nishizaka, H. Miyata, H. Yoshikawa, S. i. Ishiwata, K. Kinosita Jr, *Nature*, **1995**, 377, 251.
[235] Y.-L. Sun, Z.-P. Luo, K.-N. An, *Biochemical and Biophysical Research Communications*, **2001**, 286, 826-830.
[236] Y. Cui, C. Bustamante, *Proceedings of the National Academy of Sciences*, **2000**, 97, 127-132.
[237] Y. Takagi, E. E. Homsher, Y. E. Goldman, H. Shuman, *Biophysical Journal*, **2006**, 90, 1295-1307.
[238] M. de Messieres, J.-C. Chang, B. Brawn-Cinani, A. La Porta, *Phys. Rev. Lett.*, **2012**, 109, 058101.
[239] E. A. Abbondanzieri, W. J. Greenleaf, J. W. Shaevitz, R. Landick, S. M. Block, *Nature*, **2005**, 438, 460.
[240] A. R. Carter, G. M. King, T. A. Ulrich, W. Halsey, D. Alchenberger, T. T. Perkins, *Applied Optics*, **2007**, 46, 421-427.
[241] M. T. Woodside, P. C. Anthony, W. M. Behnke-Parks, K. Larizadeh, D. Herschlag, S. M. Block, *Science*, **2006**, 314, 1001-1004.
[242] J. Liphardt, B. Onoa, S. B. Smith, I. Tinoco, C. Bustamante, *Science*, **2001**, 292, 733-737.
[243] R. R. Brau, P. B. Tarsa, J. M. Ferrer, P. Lee, M. J. Lang, *Biophysical Journal*, **2006**, 91, 1069-1077.
[244] A. Cleland, *Nature Physics*, 2009, 5, 458.
[245] R. G. Knobel, A. N. Cleland, *Nature*, **2003**, 424, 291.
[246] J. A. Sidles, J. L. Garbini, K. J. Bruland, D. Rugar, O. Züger, S. Hoen, C. S. Yannoni, *Reviews of Modern Physics*, **1995,** 67, 249-265.
[247] M. E. Tobar, D. G. Blair, *Review of Scientific Instruments*, **1995**, 66, 2751-2759.
[248] J. C. Long, H. W. Chan, A. B. Churnside, E. A. Gulbis, M. C. M. Varney, J. C. Price, *Nature*, **2003**, 421, 922.
[249] J. Gieseler, R. Quidant, C. Dellago, L. Novotny, *Nature Nanotechnology*, **2014**, 9, 358.
[250] J. Millen, T. Deesuwan, P. Barker, J. Anders, *Nature Nanotechnology*, **2014**, 9, 425.
[251] W. Marshall, C. Simon, R. Penrose, D. Bouwmeester, *Phys. Rev. Lett.*, **2003**, 91, 130401.
[252] S. Mancini, V. I. Man'ko, P. Tombesi, *Physical Review A*, **1997**, 55, 3042-3050.
[253] S. Bose, K. Jacobs, P. L. Knight, *Physical Review A*, **1997**, 56, 4175-4186.
[254] A. D. Armour, M. P. Blencowe, K. C. Schwab, *Phys. Rev. Lett.*, **2002**, 88, 148301.
[255] C. M. Caves, *Physical Review D*, **1981**, 23, 1693-1708.
[256] T. J. Kippenberg and K. J. Vahala, *Science*, 2008, 321, 1172-1176.
[257] O. Romero-Isart, M. L. Juan, R. Quidant, J. I. Cirac, *New Journal of Physics*, **2010**, 12, 033015.
[258] J. Gieseler, B. Deutsch, R. Quidant, L. Novotny, *Phys. Rev. Lett.*, **2012**, 109, 103603.
[259] A. Ashkin, J. M. Dziedzic, *Appl. Phys. Lett.*, **1976**, 28, 333-335.
[260] A. Ashkin, J. M. Dziedzic, *Appl. Phys. Lett.*, **1977**, 30, 202-204.
[261] G. Ranjit, M. Cunningham, K. Casey, A. A. Geraci, *Physical Review A*, **2016**, 93, 053801.

[262] V. Jain, J. Gieseler, C. Moritz, C. Dellago, R. Quidant, L. Novotny, *Phys. Rev. Lett.*, **2016**, 116, 243601.
[263] T. Li, S. Kheifets, M. G. Raizen, *Nature Physics*, **2011**, 7, 527.
[264] A. Ridolfo, R. Saija, S. Savasta, P. H. Jones, M. A. Iatì, O. M. Maragò, *ACS Nano*, **2011**, 5, 7354-7361.
[265] A. A. Geraci, S. B. Papp, J. Kitching, *Phys. Rev. Lett.*, **2010**, 105, 101101.
[266] B. C. Stipe, H. J. Mamin, T. D. Stowe, T. W. Kenny, D. Rugar, *Phys. Rev. Lett.*, **2001**, 86, 2874-2877.
[267] M. S. Grinolds, WarnerM, K. De Greve, DovzhenkoY, ThielL, R. L. Walsworth, HongS, MaletinskyP, YacobyA, *Nature Nanotechnology*, **2014**, 9, 279-284.
[268] L. P. Neukirch, E. von Haartman, J. M. Rosenholm, A. Nick Vamivakas, *Nature Photonics*, **2015**, 9, 653.
[269] A. Manjavacas, F. J. Rodríguez-Fortuño, F. J. García de Abajo, A. V. Zayats, *Phys. Rev. Lett.*, **2017**, 118, 133605.
[270] R. Zhao, A. Manjavacas, F. J. García de Abajo, J. B. Pendry, *Phys. Rev. Lett.*, **2012**, 109, 123604.
[271] J. Dalibard, C. Cohen-Tannoudji, *Journal of the Optical Society of America B*, **1985**, 2, 1707-1720.
[272] M. L. Juan, M. Righini, R. Quidant, *Nature Photonics*, **2011**, 5, 349.

Figures

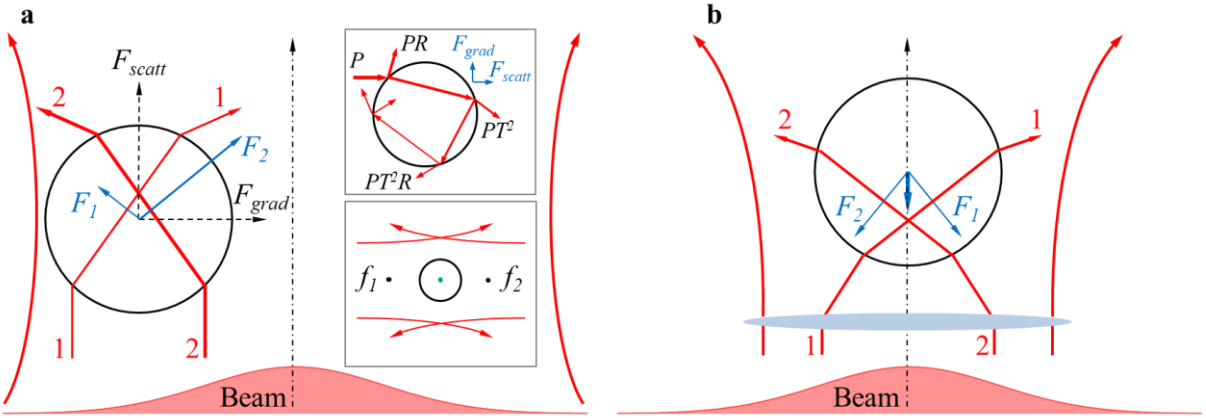

Figure 1. Origin of the scattering and gradient forces, F_{scatt} and F_{grad} for high refractive index spheres due to a Gaussian beam, in the geometrical (ray optics) regime. **a)** The forces F_1 and F_2 have longitudinal and transversal components. The formers sum up to produce the scattering force in the direction of the beam. The latters are opposite in direction and due to the lateral displacement from the beam axis, result in the gradient, restoring force which draws the particle towards the centre of the beam. Inset, top: geometry for determining the force using the Fresnel equations for reflection and transmission. Inset, bottom: geometry of two-beam trap—the scattering and gradient forces of the counter-propagating lasers lock the particle in the equilibrium point (green dot). **b)** For tightly focused rays, F_1 and F_2 produce a net force towards the beam focus.

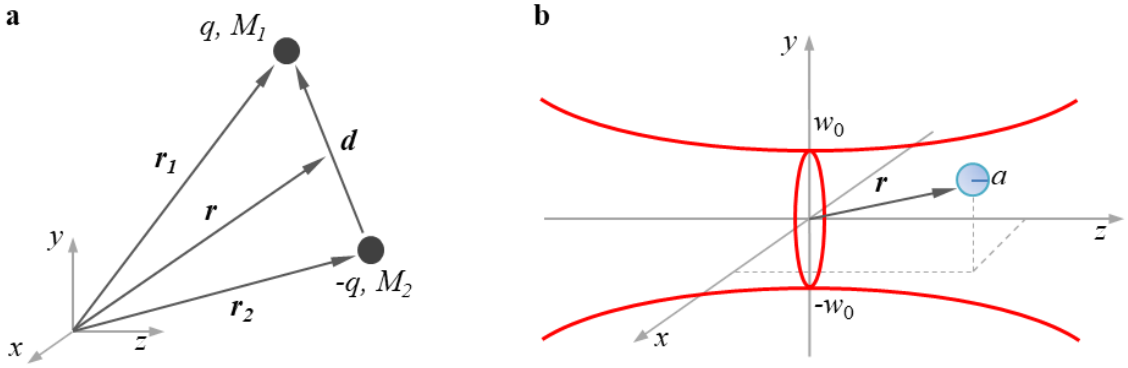

Figure 2. Schematics and conventions for deriving the optical forces in the Rayleigh regime. **a)** The trapped object is considered as a point-like dipole consisting of two particles of mass M_1 and M_2 and opposite charge, q and $-q$. The quantity **r** is the centre of mass coordinate. **b)** Geometry of a particle of radius a at position $\boldsymbol{r}$ in a Gaussian trapping beam of waist w_0.

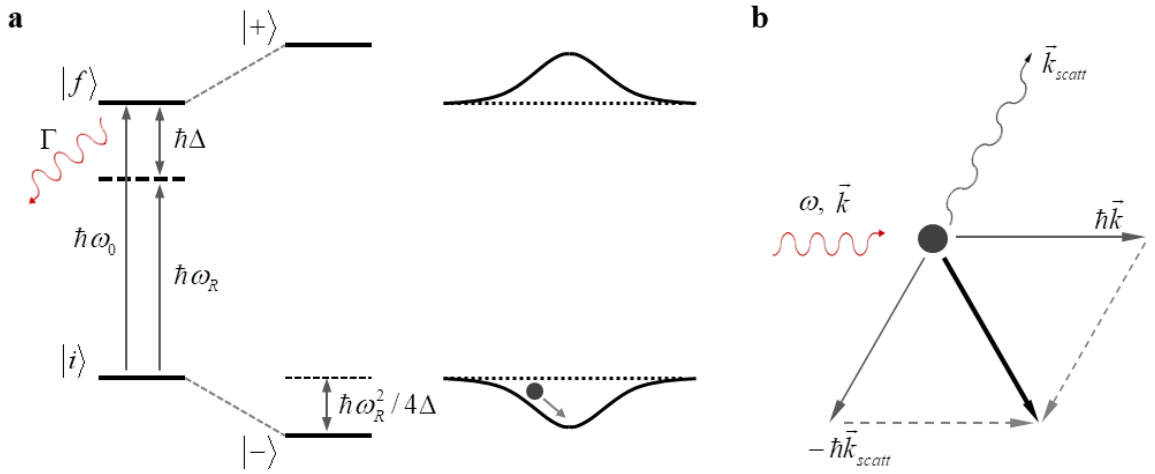

Figure 3. Gradient and scattering forces in the semiclassical description. **a) Left:** light-shifts for a two-level atom interacting with an off-resonant laser. The laser—detuned by Δ—couples to the ground and excited states $|i\rangle$ and $|f\rangle$ with Rabi frequency ω_R. The interaction causes the ground and excited states to form light-shifted dressed states[271] $|+\rangle$ and $|-\rangle$. The quantity Γ is the spontaneous emission decay rate from the excited state. **Right:** a spatially inhomogeneous field (e.g. a Gaussian laser beam) produces a ground-state potential well, in which an atom can be trapped. This mechanism is responsible for the gradient force. **b)** Momentum exchanges between the atom and photons in a single fluorescence cycle. Over many cycles, the recoil $-\hbar\vec{k}_{scatt}$ due to the spontaneously scattered photons averages out to zero: the average momentum acquired by the atom is directed along the wavevector $\vec{k}$ of the incident laser. This mechanism is responsible for the scattering force.

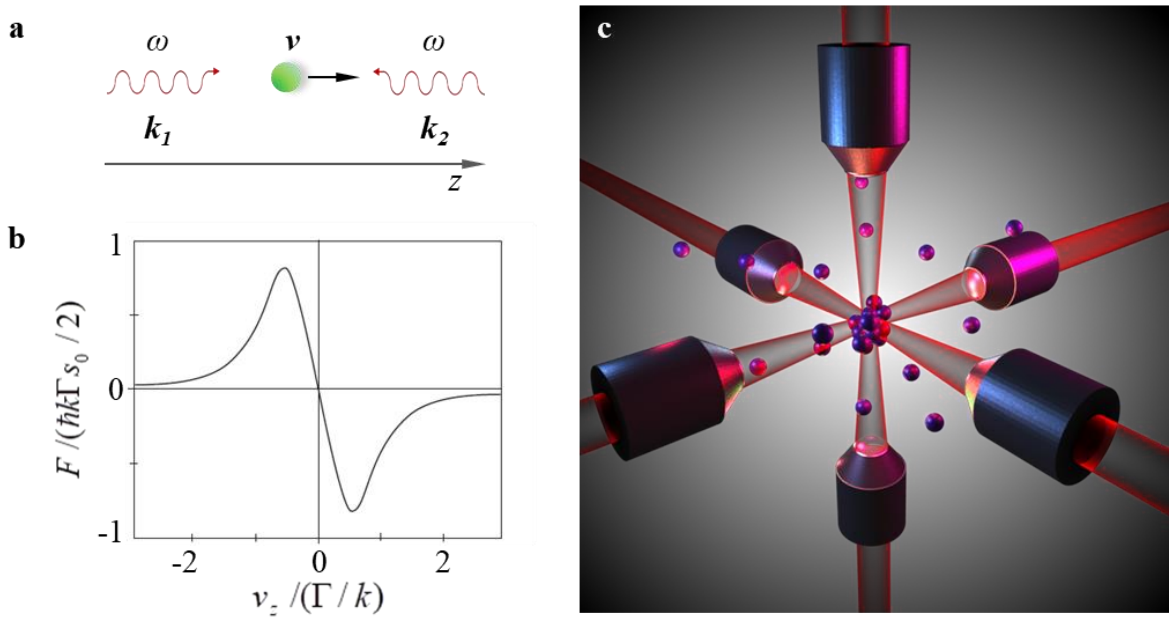

Figure 4. Doppler cooling and applications. **a)** Doppler cooling in one dimension. Two counter-propagating waves ($\vec{k}_2 = -\vec{k}_1$), are incident on the atom. They have the same intensity and frequency $\omega < \omega_0$, (ω_0 being the atomic resonance frequency). In the reference frame of the moving atom, the wave that opposes its motion is closer to resonance than the one in the direction of motion and its absorption is predominant. This slows the atom down due to conservation of momentum. **b)** Resultant force of the two waves in (a), plotted in reduced units ($\hbar k \Gamma s_0 / 2$, with $s_0 = I / I_{sat}$), and for $\delta = -\Gamma / 2$. The total radiative force always opposes the velocity of the atom (friction-type force). An ensemble of atoms with initial velocities $\sim \Gamma / k$ is efficiently cooled. **c)** Three pairs of counter-propagating laser beams along three orthogonal axes can slow down atoms in all spatial directions (figure not to scale).

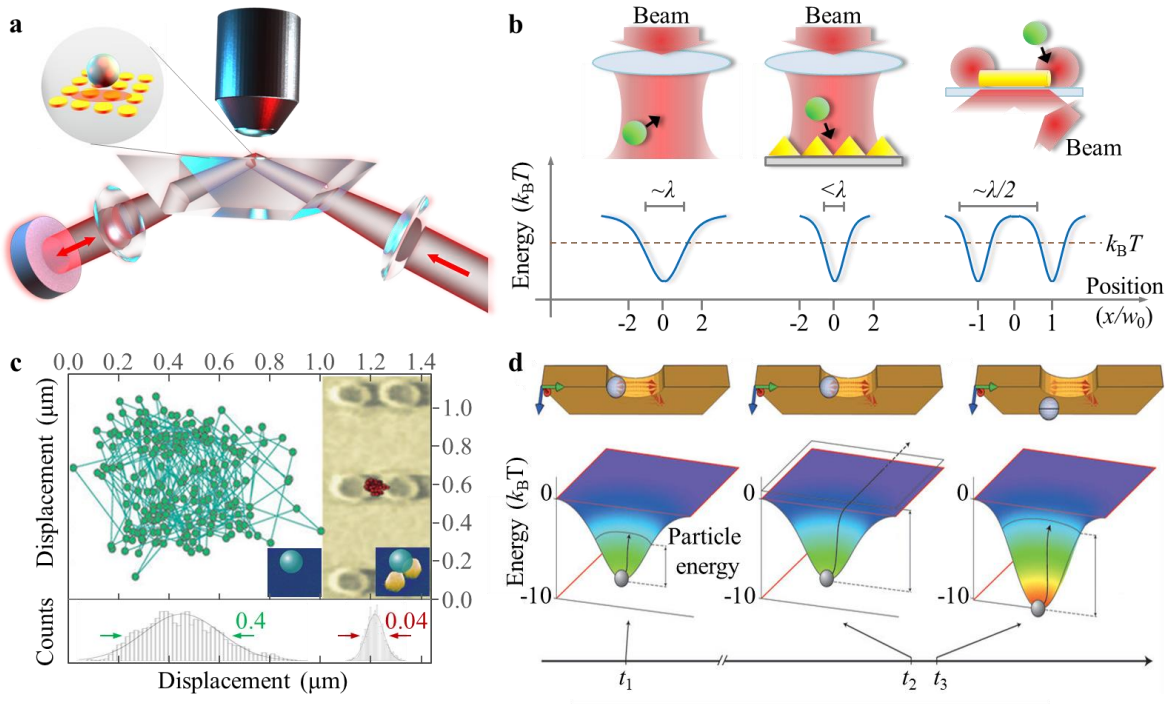

Figure 5. Plasmonic optical tweezers: basic designs and performance. **a)** Schematic of the Kretschmann configuration. The laser beam is guided through a prism. Evanescent optical waves are excited at the interface between a high (glass prism) and a low (water) refractive-index medium; the beam is incident at the total-internal-reflection angle. Plasmonic structures such as nanopillars, nanoholes, nanopyramods, etc. (inset) are used to create high local fields confined in a sub-diffraction volume and able to efficiently trap nanoparticles. A microscope objective, atop, is used to image the sample. **b)** Comparison of designs and performances for conventional (left) and plasmonic optical tweezers (centre, right). Notice how POTs are exploited to create more localised and intense fields than their conventional OTs counterpart. In POTs the linear size of the trap can break the diffraction limit, with specific designs (right) offering dramatic confinement. Note: drawings are not to scale and depths of the potential can change based on size and properties of the nanoparticles—scales of reference are approximate. **c)** First demonstration by Grigorenko et al. that a 200-nm nanoparticle held by conventional OTs is confined more efficiently—owing to plasmon resonances—when it is between two metallic nanodots (red circles) rather than free (green circles). The histograms at the bottom

show the distribution of the displacement for the two cases, fitted with Gaussians. **d)** Schematic of self-induced back-action (SIBA) POTs. The particle is localized in the aperture with a certain kinetic energy at time t_1 (left). Upon a high-energy event at time t_2, the object starts leaving the trap (centre). As the particle is moving out of the aperture at time t_3, the SIBA force increases the potential depth and keeps the object within the trap. Figures adapted and reproduced with permission (c),[80] 2008, Springer Nature; (d),[272] 2009, Springer Nature.

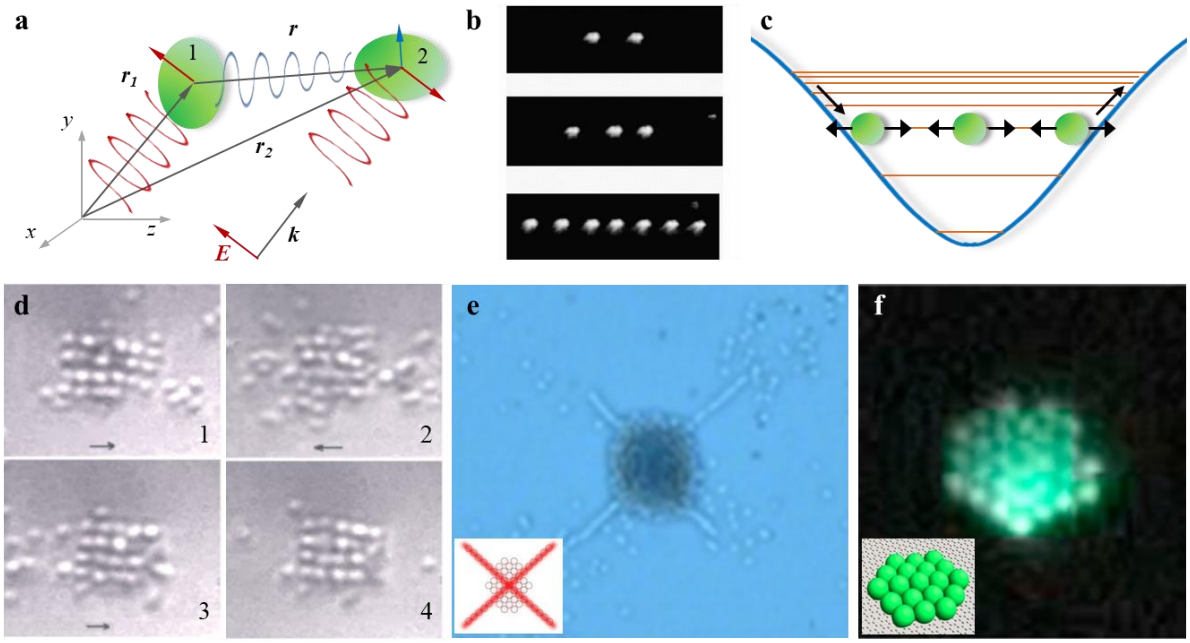

Figure 6. Optical binding. **a)** Simplified schematic representation of the optical binding mechanism (for the electric field component) between two particles, assuming absence of multiple scattering. The incident field (red wavy lines) induces the dipoles $\boldsymbol{p}_j(\boldsymbol{r}_j) = \alpha_j \boldsymbol{E}(\boldsymbol{r}_j)$, with j = 1, 2 on particle '1' and '2', respectively (red arrows centred at particles '1' and '2'). The field emitted by particle '1' (blue wavy line) reaches particle '2' and induces the dipole component (blue arrow centred at particle '2') $\boldsymbol{p}_{1\text{-}2}(\boldsymbol{r}_1) = \mathbf{G}\alpha_1 \boldsymbol{E}(\boldsymbol{r}_1)$ which interacts with the incident field $\boldsymbol{E}(\boldsymbol{r}_2)$. The quantity **G** is the field propagator (or dyadic Green's function) between two dipoles.[106] **b)** Linear arrays of two (top), three (centre) and seven (bottom)

polystyrene spheres (diameter 3 μm) in water, achieved via optical binding, between the foci of two counterpropagating beams. **c)** Diagrams showing the filling up of the approximately harmonic potential created by the two counterpropagating beams in (b) for the case of three spheres. **d)** Image of a 2D- and 3D-optical crystal (as it assembles: 1 through 4) by means of sets of crossed beams. The particles are 490-nm-diameter polystyrene spheres in water. Arrows indicate the areas where the lattice potential is deepest. **e)** Optical trapping and assembly of nanoparticles in a complex horn-like structure, exploiting optical binding and light polarization. Inset: schematic of laser intensity (red lines) relative to the particles. **f)** Optical micrographs and model (inset) of a closely-packed assembly of 500-nm polystyrene nanoparticles via metal nanostructures. Figures adapted and reproduced with permission: (b),[109] 2002, APS Physics; (d),[113] 2011, APS Physics; (e),[117] 2016, ACS Publications; (f),[119] 2011, ACS Publications.

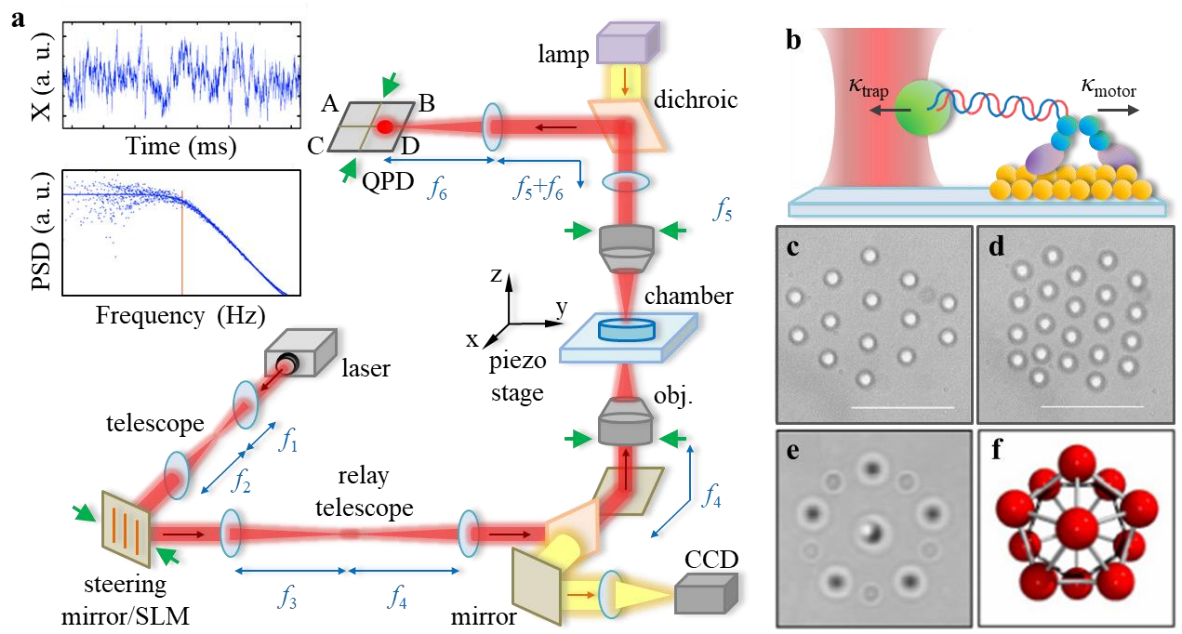

Figure 7. Design for conventional OTs and applications. **a)** Schematic of conventional OTs. The beam telescope, steering mirror and relay telescope send the laser to slightly overfill the back aperture of the high-NA trapping objective, which focuses the beam into the chamber.

Direct imaging of the sample is possible with a CCD camera, whereas tracking is carried out with a quadrant photodiode (QPD). Lenses are precisely positioned to assure that the beam can be manipulated without walking at the objective back aperture: this allows moving the trapping position of the beam in the sample plane without significant power losses. The small green arrows indicate conjugated planes. (Note: for HOTs the steering mirror is replaced by a spatial light modulator, SLM). Insets: time tracking and corresponding power spectrum density (PSD; the red line indicates the corner frequency) of the particle in the OT. **b)** Schematic representation of force clamps in single-bead configuration to measure the motion of the molecular motor kynesin. The quantity κ_{trap} is the trap stiffness, while κ_{motor} comprises the motor protein stiffness in series with the stiffness of the linkages connecting the protein to the bead and the coverslip surface (note that the bead is also subject to the Stokes drag coefficient β). **c, d)** Silica particles (size 1.5 μm) trapped in water using a scanning laser optical trap. Scale bar is 10 μm. **e, f)** Image (e) and corresponding geometry schematics (f) of a rotating icosahedron of colloidal spheres (size 1.5 μm) created with dynamic holographic optical tweezers. Figures adapted and reproduced with permission (c, d),[150] 2001, Elsevier; (e, f),[160] 2005, OSA Publishing.

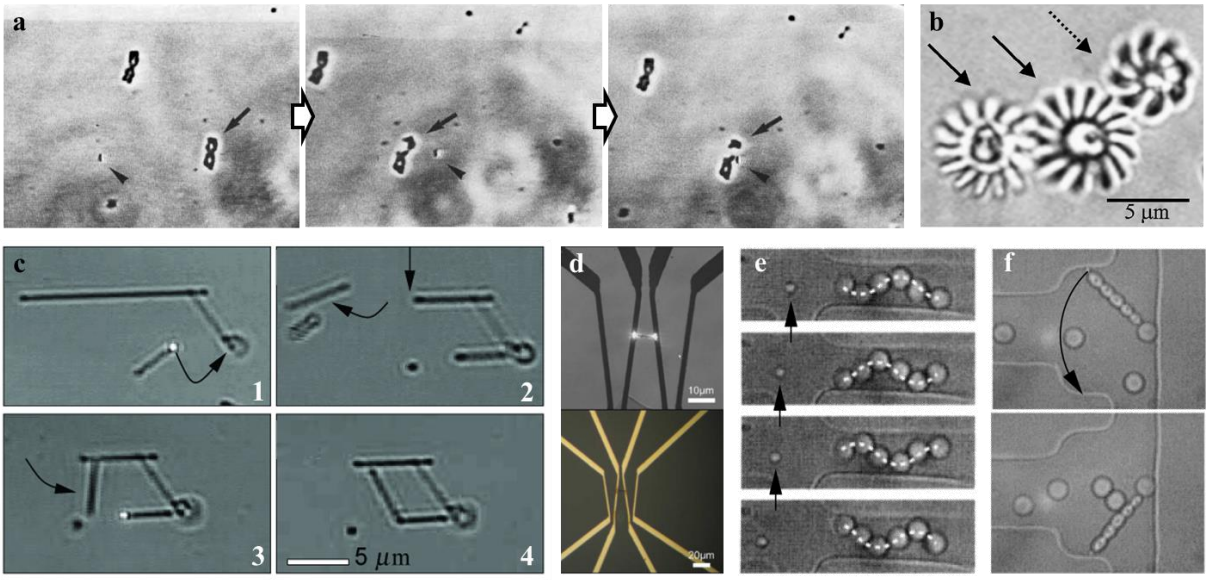

Figure 8. OTs Applications: nanoassembly and actuation. **a)** Microdissection using OTs and a UV cutting laser. A single chromosome (black arrow) adherent to the glass coverslip is selected (left); a UV laser (black triangle) cuts it into segments (centre); by radiation pressure, a second, trapping laser (at 1,064 nm) detaches the chromosome from the glass away from the cut telomere (right). **b)** Complex micromachine built by photopolymerization, and actuated by OTs. Two engaged cogwheels (solid arrows) are rotated by a light-driven rotor (dashed arrow) which is held and spun by the laser tweezers. **c)** Assembly of a rhomboidal structure from semiconductor nanowires using HOTs. A nanowire is brought to an existing structure created earlier by trapping and fusing two nanowires (1). The long nanowire is cut with a pulsed optical scalpel (2). The resulting free-floating nanowire piece is then brought back to the structure and fused to the fourth nanowire (3, 4). **d)** Fusion of nanowire onto a premade structure. OTs are used to bring a nanowire to the target site and fuse it to a preexisting, imprinted Au electric circuit. **e)** Silica beads (~3 μm) activated by optical trapping and used as a peristaltic pump, operating at 2 Hz, to push a 1.5-μm tracer sphere (arrow) in water solution. **f)** Silica beads (one 3-μm in size, working as the fulcrum, and five 0.64-μm in size, working as the arm) assembled by photopolymerization via optical trapping into a three-way valve. The same trapping laser used to assemble the spheres into the valve is also used to actuate it and sort 3-μm beads with flow rates of ~2 $nl \cdot h^{-1}$. Figures adapted and reproduced with permission: (a),[201] 1991, Wiley; (b),[207] 2001, AIP Publishing; (c),[218] 2005, OSA Publishing; (d),[219] 2009, OSA Publishing; (e, f), [222] 2002, AAAS;

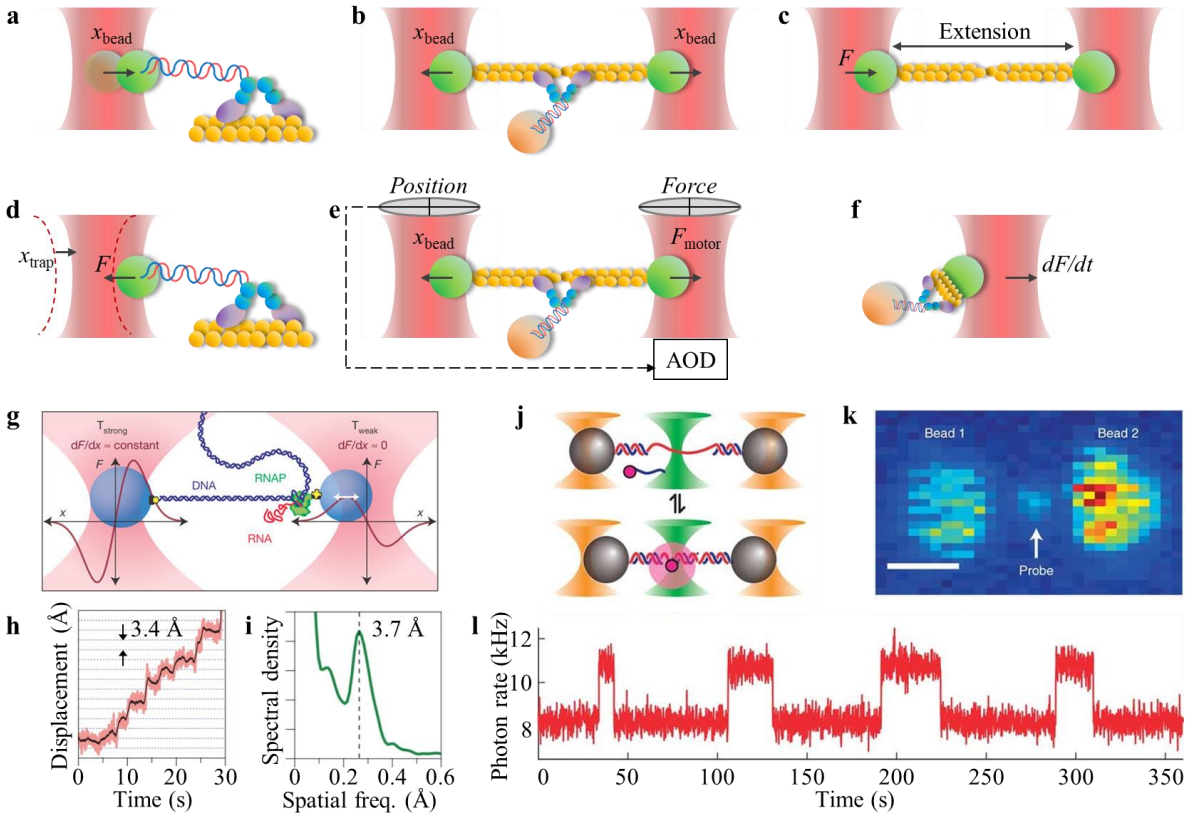

Figure 9. OTs Applications: force and displacement measurement in biology. **a)** Single-bead geometry. The laser trap is static and the protein displacement is measured via the bead position (x_{bead}). **b)** Three-bead geometry. Both laser traps are static, the protein displacement is measured via the trapped beads position (x_{bead}). **c)** Two-bead geometry. The left trap is static and measures the force applied to the polymer. The right bead is moved in steps or ramps and the forces of the polymer extension are measured. **d)** Force-clamps. A feedback tracking mechanism moves the laser trap to maintain the force on the bead constant. Protein displacements are measured by trap position (x_{trap}). **e)** Position-clamps. The left bead detects movements of the dumbbell (x_{bead}), whereas the right bead moves using an acousto-optic deflector (AOD) to oppose the measured movements. The right bead measures the force applied by the motor (F_{motor}). **f)** Dynamic force spectroscopy. The molecular bond is subjected to constant loading rates; rupture forces and bond lifetimes are measured. **g–i)** Measurement of base-pair stepping during RNA polymerase (RNAP) action via two-bead, optical force clamps. In the schematic (g), a single transcriptionally active molecule of RNAP (green) is

attached to a bead (blue) held in the trap to the right (T_{weak}) and tethered via the upstream DNA (dark blue) to a larger bead held in the trap to the left (T_{strong}). During elongation, the DNA tether lengthens; the right bead moves relatively to the left one and its displacement is measured. Representative record (h) for single molecules of RNAP transcribing <18 pN of assisting load—median-filtered at 50 ms (pink) and 750 ms (black). The horizontal dotted lines are spaced at 3.4 Å intervals. The graph in (i) is the power spectrum showing a peak at the dominant spatial frequency, corresponding to the inverse of the fundamental step size of (3.7 ± 0.6) Å. **j–l)** Schematic of dual optical trap combined with a confocal microscope. Two beads are held in dual traps tethered together by 3-kbp dsDNA with a 19-nt single-stranded portion near the centre. The ssDNA probe strands diffuse in the surrounding solution and bind-unbind the complementary single-stranded region in the tethered DNA (j). Fluorescence image with the probe bound to the tethered DNA labeled. Scale bar, 1 μm (k). Plot of fluorescence with the confocal measurement localized between the two beads at the probe strand binding location. Fluorescence increases and decreases as the probe binds and unbinds, respectively (l). Figures adapted and reproduced with permission: (a–f),[137] 2013, Elsevier; (g–i),[239] 2005, Springer Nature; (j–l),[183] 2011, Springer Nature.

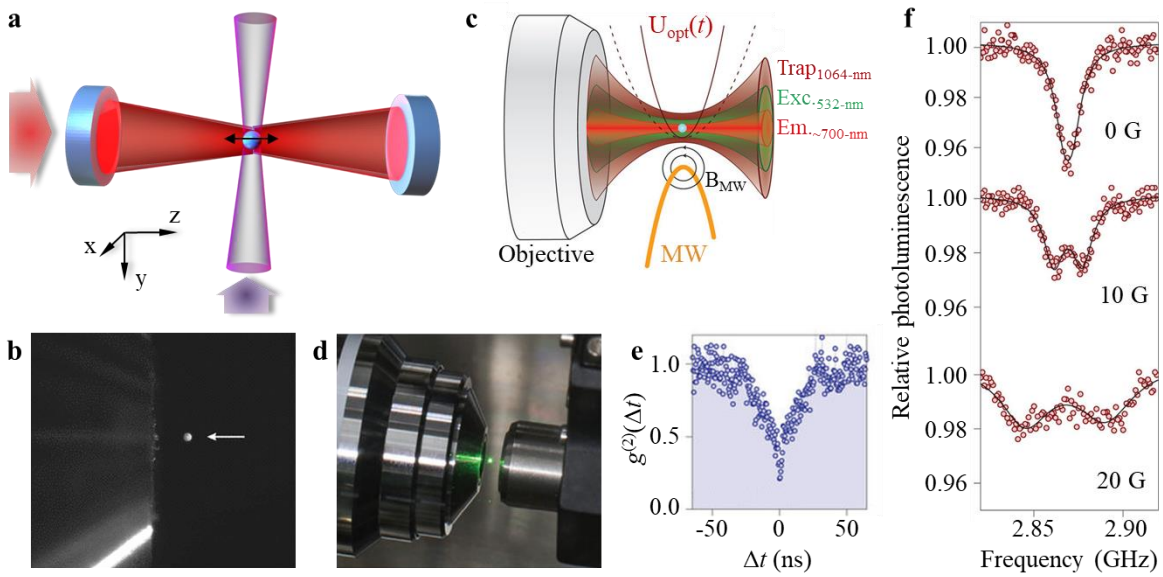

Figure 10. OTs applications: optomechanics. **a)** A dielectric sphere is trapped by OTs inside a high-finesse optical cavity. The confinement of the centre-of-mass motion along the z-axis is harmonic. The driving field generates radiation pressure to cool down the mechanical motion to the ground state. **b)** Photograph of light scattered from an optically-trapped, levitating silica nanoparticle (size ~70 nm, arrow), in high vacuum. The object to the left is the outline of the objective that focuses the trapping laser. **c)** Schematic of an optical trap to levitate a diamond nanoparticle (size ~100–150 nm) containing a single nitrogen-vacancy (NV) colour centre. The trapping laser (wavelength at 1,064 nm) is superimposed to a green laser (wavelength at 532 nm) and emission from the NV centre (wavelength ~637–750 nm) is collected. A microwave field (MW) and a magnetic field (B_{MW}) are applied to measure the optically detected magnetic resonance (ODMR) spectrum from the NV (f). **d)** Photograph of the levitated nanodiamond illuminated by the green laser in (c). **e)** Second order auto-correlation measurement showing that the levitated nanodiamond in (c) contains a single NV quantum emitter ($g^{(2)}(\Delta t) < 0.5$ at $\Delta t = 0$). **f)** ODMR spectrum of the NV centre hosted in the levitated nanodiamond in (c). The microwave field pumps the NV from its (bright) ground spin state $m_s = 0$ to the (dark) ground spin states $m_s = \pm 1$. The magnetic field splits the degeneracy of the levels $m_s = +1$ and -1 by an amount proportional to the intensity of the field. The overall experiment in (c) demonstrates the ability to imprint the multi-dimensional mechanical motion of the cavity-free mechanical oscillator into the nitrogen–vacancy (NV) centre fluorescence and manipulate the mechanical system's intrinsic spin. Figures adapted and reproduced with permission: (b),[258] 2012, APS Physics; (c–f),[268] 2005, Springer Nature.

Biography – Dr Carlo Bradac

Dr Carlo Bradac is a Research Fellow at the University of Technology, Sydney (AU). He received his Bachelor (2004) and Master degree (2006) in Engineering for Physics and Mathematics at the Polytechnic of Milan (IT). He worked as an Application Engineer (2006–2007) and as a Process, Control & Automation Engineer (2007–2008). He received his PhD in Physics at Macquarie University (Sydney, AU) in 2012, and worked as a Research Fellow at Sydney University (2012–2013), Macquarie University (2013–2017) and the University of Technology of Sydney (2017–Current). His research focuses on solid-state quantum optics, photonics and biomedicine.

Optical trapping is the craft of manipulating objects with light. A powerful, well-established tool for ultracold-atom physics and manipulation of micron-sized particles, optical trapping of objects at the nanoscale is still confronting open challenges. These are presented alongside the state-of-the-art of the field and its potential for advancing future applications in single-molecule biology, hybrid-device nanofabrication and quantum-driven optomechanics.

Keywords: optical tweezers, optical trapping, optical forces, nanostructures

C. Bradac*

Nanoscale Optical Trapping: a Review